Clay Minerals (2024), **59**, 228–257
doi:10.1180/clm.2024.17

CAMBRIDGE UNIVERSITY PRESS

Review Article

Climatic significance of clay minerals in Cenozoic marine and lacustrine sediments

Nathalie Fagel
Laboratory AGEs ('Argiles, Géochimie et Environnement sédimentaires'), Département de Géologie, Université de Liège, Liège, Belgium

Abstract

In sediments, clay minerals are mainly detrital. Formed by continental weathering, they are carried by surface transport predominantly by rivers, glaciers and, to a lesser extent, winds to the adjacent sedimentary basins and then are redistributed by oceanic currents. In a sedimentary core, the variability in the clay mineral assemblages reflects either variable physical and chemical weathering conditions in the watershed, typically with a significant link to climatic conditions, or changes in the mineral source, the latter being associated with various transport agents. When different sources are involved, a combination of mineralogical and geochemical proxies allows us to trace the detrital provenance, but they also indirectly provide valuable information on transport pathways and palaeocurrents. This manuscript reviews several examples from the literature and ongoing research on clay mineral variability in marine or lacustrine sedimentary records and interprets them in terms of: (1) climate control at different timescales, from the Neogene to the Quaternary; and (2) transport paths. Examples are selected to review the various clay-derived proxies in existence.

Keywords: Cenozoic, clay-derived proxy, climate lake, ocean, provenance, Quaternary, sedimentary cycle

(Received 20 October 2023; revised 14 June 2024; Associate Editor: Javier Cuadros)

Introduction

The clay toolbox

Palaeoclimate reconstructions are derived from the interpretation of temporal series of various sedimentary proxies (e.g. fauna, flora, mineralogy, chemistry, isotopic composition). However, most palaeoreconstructions concern the evolution of temperatures, whereas reconstructions of humidity conditions are scarce. Besides pollen assemblages, clay minerals are the only proxy used to derive hydrological conditions (i.e. hydrolysis conditions during pedogenesis and runoff; e.g. Munier *et al.*, 2021). Hydrolysis represents the principal chemical weathering process, and it consists of the attack of rocks by water of low ion content under medium pH (Chamley, 1989).

Sedimentary clay minerals can be a powerful climate proxy (Fig. 1) if they fulfil two main requirements (Fagel, 2007). First, clay minerals must be detrital in origin, representing either primary (inherited clay) or secondary products (Chamley, 1989; Ruffel *et al.*, 2002). Primary clay minerals are inherited from parental rocks by physical weathering. Most frequently, these clay minerals are represented by illite and chlorite. However, in principle, any clay mineral can be reworked into a rock that may then be eroded and weathered in a new cycle. Secondary clay minerals result from chemical weathering processes, mainly hydrolysis, occurring on the rock surface and in soils, formed by progressive transformation of a mineral precursor (i.e. silicate mineral into smectite) or by a recombination of ions in a confined environment (i.e. kaolinite neoformed from Al-rich rocks). Second, clays must not be significantly altered by burial diagenesis.

In most cases, the geochemical signature of the clays allows us to distinguish between detrital clay minerals of continental origin and authigenic clays formed by chemical precipitation from a saturated solution under surface conditions (Deocampo *et al.*, 2010) or related to hydrothermal circulation (Alt & Jiang, 1991; Fagel *et al.*, 1992a; Inoue, 1995). The influence of diagenesis can be detected through the progressive evolution of clay mineral assemblages over burial depth (Dunoyer de Segonzac, 1969; Perry & Hower 1970; Peacor, 1992; Kemp *et al.*, 2005), which results in a simplified mineral assemblage dominated by illite and/or chlorite (e.g. Chamley, 1989; Meunier, 2006).

Establishing climate input in detrital sedimentary clays is best done by identifying the source areas and the principal transport agents. The mineralogical and geochemical (trace elements and radiogenic isotopes) composition of the sedimentary clays may be compared with the average composition of clays from the adjacent surroundings to identify the main continental source areas (Fagel *et al.*, 1997a, 2002, 2004), which also enables indirect identification of transport agents (e.g. Fagel *et al.*, 1999). This combined approach was described in Fagel (2007).

Sedimentary material

From the 1960s, down-core variations in marine clay mineral assemblages have been interpreted in terms of changes in the climate conditions prevailing in the continental source areas (Warr *et al.*, 2022) and have been widely used to reconstruct palaeoclimates (e.g. Millot, 1970; Singer, 1984; Chamley, 1989). The clay mineral-derived proxy was set from the latitudinal, climate-driven clay mineral distribution trends observed in deep-seafloor sediments of the Pacific Ocean (Griffin & Goldberg, 1963), the Atlantic Ocean (Biscaye, 1965; Petschick *et al.*, 1996),

Email: nathalie.fagel@uliege.be
Cite this article: Fagel N (2024). Climatic significance of clay minerals in Cenozoic marine and lacustrine sediments. *Clay Minerals* **59**, 228–257. https://doi.org/10.1180/clm.2024.17

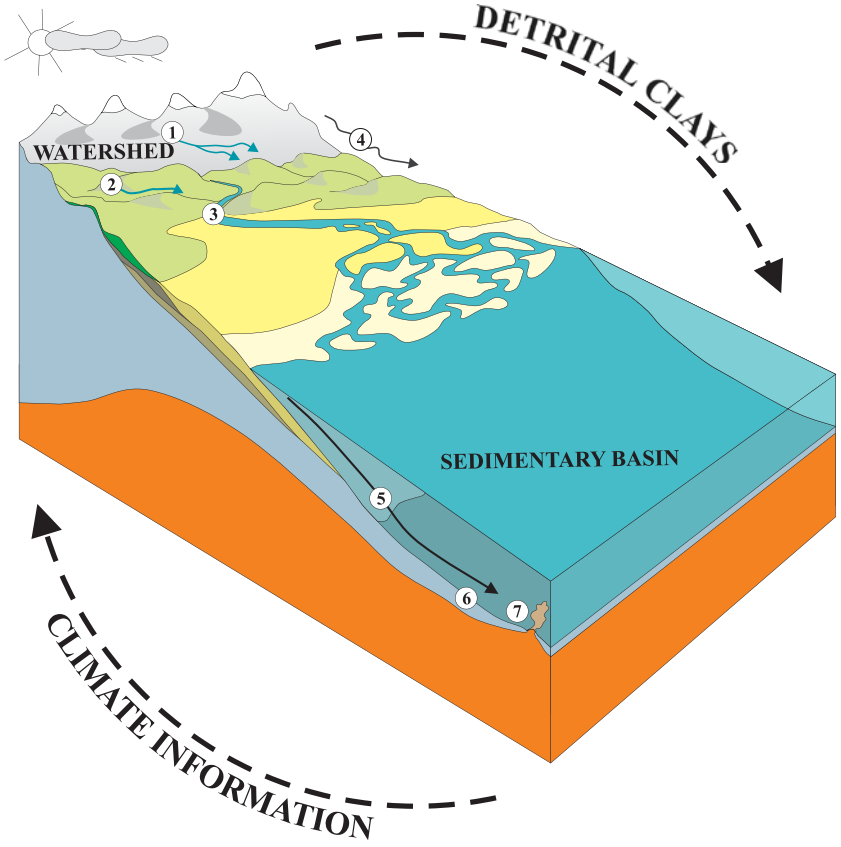

Figure 1. The clay toolbox to obtain past climatic information from detrital clay minerals (modified from Fagel, 2007). The numbers indicate different steps of the sedimentary cycle. (1) Physical weathering delivers primary clay minerals (typically illite and/or chlorite) by mechanical disaggregation of parental rocks outcropping in the watershed. (2) Chemical weathering produces secondary clay minerals in soils either by transformation of primary minerals (smectite) or neoformation by recombination of cations (kaolinite). Weathering products are eroded and transported by rivers (3), wind (4) or glaciers (5) to the adjacent sedimentary basin (i.e. a lake or an oceanic basin). The weathering products are carried by underwater currents and settle down as a sedimentary deposit (6) at the bottom of the water column when the current velocity decreases. Sedimentation causes partial separation of clay minerals according to particle size. In addition, authigenic clay minerals may be formed by hydrothermal or volcanic activity at the ocean floor (7).

the Indian Ocean (Kolla *et al.*, 1976) or even worldwide (e.g. Griffin *et al.*, 1968; Rateev *et al.*, 1969; Windom, 1976). Later, the relationship between clay minerals and seafloor bathymetry emphasized the impacts of intermediate and/or deep oceanic circulation on the distribution of detrital clay minerals in surface sediments (Petschick *et al.*, 1996; see Fagel, 2007 for a review).

Over the last decade, the significance of climate for the evolution of clay mineral assemblages has been emphasized in many studies of marine sediments. A few studies have also been performed in lake settings. Whatever the environment, the climate interpretation is derived from the evolution of potential clay proxies over core depth or time. The most common proxy corresponds to the ratio between the relative abundance of at least two clay minerals (e.g. kaolinite/chlorite (Biscaye 1965; Petschick *et al.*, 1996) or smectite/illite (e.g. Sakai *et al.*, 2005)), although, in some cases, the abundance of one only clay mineral (e.g. palygorskite; Bout-Roumazeilles *et al.*, 2007) was also used. Examples of clay proxies and their interpretation in terms of climate or other factors are reported in Tables 1 & 2 for marine and lacustrine settings, respectively. This manuscript presents an overview of studies using clay mineral assemblages as proxies for climate variability in marine or lacustrine records (Fig. 2). It is emphasized that sedimentary clay minerals may record climate variability at different timescales and therefore may represent suitable proxies for palaeoclimate reconstructions.

Limitations of the clay mineral proxy

Only the detrital clays that are not affected by burial diagenesis may be used for palaeoclimate reconstructions. Moreover, the use of detrital clay minerals as climate proxies is mainly only valid for Cenozoic sediments. For Palaeozoic series, the palaeoclimate information is in most cases erased by burial diagenesis (e.g. Han *et al.*, 2000; Hillier *et al.*, 2006) that transformed the diversified clay mineral assemblages in simplified assemblages dominated by illite and chlorite (e.g. Chamley, 1989; Meunier, 2006). The Mesozoic was marked by limited orogenic activity on the continents and warm climatic conditions (i.e. greenhouse period; Chandler *et al.*, 1992; Fletcher, 2008; Korte *et al.*, 2015; Landwehrs *et al.*, 2021). Both conditions reduced the detrital supplies and favoured a biogenic sedimentation marked by carbonates and marls (e.g. Hesselbo *et al.*, 2013; Munier *et al.*, 2021). Assuming a negligible effect of burial diagenesis, the variations in clay mineral assemblages on outcrops or boreholes were used to reconstruct climate conditions during the early Jurassic (Kemp *et al.*, 2005; Jeans, 2006; Dera *et al.*, 2009; Hesselbo *et al.*, 2020, Munier *et al.*, 2021), the middle and late Jurassic (e.g. Pellenard & Deconninck, 2006; Huang *et al.*, 2010) or the Cretaceous (e.g. Schnyder *et al.*, 2006; Godet *et al.*, 2008). Unlike the Mesozoic, the Cenozoic sedimentation is characterized by high detrital fluxes supplied by physical erosion enhanced by tectonic uplift related to the Alpine orogenesis since the Oligocene (e.g. Zachos *et al.*, 2001; Schlunegger & Norton, 2015). The detrital mineral supplies are also enhanced by climate trends, marked by a global cooling over the Cenozoic (Zachos *et al.*, 2001). Moreover, some detrital clays may be reworked from past sedimentary outcrops. Such clay minerals may not be useful for climate reconstructions, as the time between the initial formation of the clay mineral (in the previous erosion cycle) may be long and the climate conditions may have changed over time (Thiry, 2000). For instance, the widespread occurrence of kaolinite in Quaternary sediments of the Arctic Ocean was explained

Table 1. Examples of studies using clay mineral-derived proxies from Neogene to Quaternary sedimentary records retrieved by coring in oceanic basins.

Clay proxy	Location	Project	Site	Latitude	Longitude	Water depth (m)	Age interval	Interpretation	Reference(s)
Palygorskite/illite	Owen Ridge (Arabian Sea)	ODP117	721B	16°41'N	59°52'E	1935	2.7–1.2 Myr	Orbital control on Indian monsoon	Fagel *et al.* (1992b)
Bulk mineralogy	Owen Ridge (Arabian Sea)	ODP117	722B	16°37'N	59°48'E	2022	Last 500 kyr	Variable weathering conditions in source area	Krissek & Clemens (1991)
Clay mineralogy	Bengal Fan (north-east Indian Ocean)	DSDP22	218	08°00'N	86°17'E	3737	Last 185 kyr	Intensity of chemical weathering over glacials/interglacials	Bouquillon *et al.* (1989)
		ODP116	717C	00°56'S	81°23'E	4735	Last 17 Myr	Provenance: smectite from Indo-Gangetic Plain, illite and chlorite from Himalayas	Bouquillon *et al.* (1990)
		ODP116	718C	01°01'S	81°24'E	4731			
Smectite/(illite + chlorite)	Bengal Fan (north-east Indian Ocean)	MD77-180		18°28'N	89°51'E	1986	Last 240 kyr	Variable intensity of chemical weathering, orbital control related to south-west monsoon	Colin *et al.* (1999)
		MD12-3412		17°11'N	89°29'E	2368	Last 180 kyr	Variable weathering conditions over glacials/interglacials	Joussain *et al.* (2016)
Clay mineralogy	Andaman Sea (north-east Indian Ocean)	BoB-56		16.56°N	88.55°E	2615	Last 40 kyr	Variable monsoon over glacials/interglacials	Li *et al.* (2018)
Smectite/(illite + chlorite)	Andaman Sea (north-east Indian Ocean)	MD77-169		10.8°12'N	95°03'E	2360	Last 280 kyr	Intensity of chemical weathering, orbital control related to south-west monsoon	Colin *et al.* (1999)
Smectite/(illite + chlorite)	Central Indian Basin	MD90-947		01°24'S	76°37'E	4781	Late Pliocene	Variable weathering conditions on Indo-Gangetic Plain	
Illite–smectite	Central Indian Basin	MD90-946		03°16'S	78°01'E	4796	6.5–5.7 Myr	Climate control by eccentricity	Fagel *et al.* (1994)
Illite–smectite	Central Indian Basin						4.7–1.2 Myr	Tectonic control	
Clay mineralogy	Central Indian Basin	MD90-944		06°39'S	80°07'E	4902	Late Miocene	Variable weathering conditions on Indo-Gangetic Plain	
Illite–smectite	Central Indian Basin	MD90-943		08°19'S	79°49'E	5249	5.6–5.0 Myr	Climate control by eccentricity	
Illite–smectite	Central Indian Basin						5.1–4.3 Myr	Tectonic control	
Clay mineralogy	Central Indian Basin	MD90-942		10°03'S	79°48'E	5356	Mid-Pliocene	Variable weathering conditions on Indo-Gangetic Plain	
Bulk mineralogy	Ionian Sea (Mediterranean)	ODP160	964A	36°16'N	17°45'E	3658	3.0–2.8 Myr	Variable aridity conditions	Foucault & Mélières (2000)
Illite–kaolinite	Ionian Sea (Mediterranean)	ODP160	964	36°16'N	17°45'E	3658	Last 1500 kyr	Variable latitude of dust sources with migration of inter-tropical convergence zone	Zhao *et al.* (2012, 2016)
% palygorskite	Alboran Sea (Mediterranean)	ODP161	976	36°12'N	4°19'E	1108	Last 50 kyr	Increase of aridity and intensification of winds during North Atlantic cold events	Bout-Roumazeilles *et al.* (2007)
	Distal Nile fan (Mediterranean)	MD90-964		33°16'N	17°45'E	1375	Last 1800 kyr	Variable dust over glacials/interglacials	Zhao *et al.* (2012)
% smectite, % illite, crystallinity	Chilean Margin (Pacific)	GIK17748-2		32°45'S	72°02'W	2545	Last 15.6 kyr	Variable weathering conditions and provenance/migration of south-westerly winds	Lamy *et al.* (1999)
		GeoB3302-1		33°13'S	72°06'W	1498	28.0–9.6 kyr		
Smectite/(illite + chlorite)	SCS	ODP184	1145	19°35'N	117°38'E	3176	450 kyr	Variable intensity of East Indian monsoon, orbital control	Boulay *et al.* (2003)
		ODP185	1146	19°27'N	116°16'E	2092	Last 2 Myr	Orbital control on East Asian monsoon	Liu *et al.* (2003)

(*Continued*)

Table 1. (*Continued.*)

Clay proxy	Location	Project	Site	Latitude	Longitude	Water depth (m)	Age interval	Interpretation	Reference(s)
Clay mineralogy	Japan Sea	ODP127	794	40°11'N	138°15'E	2825	Mid-Miocene–Quaternary	Chlorite-rich assemblage related to rifting during Middle Miocene	Fagel *et al.* (1992a)
		ODP127	795	44°00'N	138°53'E	3374		Illite and chlorite increase related to convergence during Plio-Quaternary	
		ODP127	797	38°37'N	134°33'E	2495	Early Miocene–Quaternary	Chlorite-rich assemblage related to rifting during Middle Miocene	
Clay mineralogy	Arctic Ocean	HLY0503	12MC8	83°18'N	171°55'N	1586	Last 250 kyr	Variable supplies by Trans Polar Drift *vs* Beaufort gyre over glacials/interglacials	Fagel *et al.* (2014)
	North-west Atlantic, Carolina Slope	ODP172	1055	32°47'N	76°17'W	1799	Last 30 kyr	More advection of clays by deep currents during Holocene	Adkins *et al.* (1995)
							Last 59 kyr	Holocene resuspension of clay and focusing by deep water mass	Cagatay *et al.* (2002)
	North-east Atlantic, continental slope	ODP175	1085	29°22'S	13°59'E	1713	Late Mioene–early Pliocene	Kaolinite supplies by increased North Atlantic deep water between 6.9 and 5.9 Myr	Robert *et al.* (2005)
	North-west Atlantic, upper rise	DSDP93	604	38°43'N	72°33'W	2361	Late Pliocene–Pleistocene	–	Dunn *et al.* (1987)
	North-west Atlantic	SU90-11 SU90-16		44°43'N 58°13'N	40°15'W 45°10'W	3645 2100	Last 240 kyr Last 45 kyr	Evolution of deep current over glacial and interglacial periods	Bout-Roumazeilles (1995)
	North-west Atlantic, slope	ODP150	903	38°56'N	72°49'W	444	Eocene–Pleistocene	Less hydrolysis due to global cooling and tectonic uplift related to the Appalachians	Deconinck & Vanderaveroet (1996)
	North-west Atlantic, upper rise		905	38°37'N	72°17'W	2698	Middle Eocene–Holocene	Influence of southwards marine current along slope	
Illite–vermiculite mixed layers	North-west Atlantic, upper slope	Various coring sites					Pleistocene	Current transport of illite–vermiculite mixed layers from northern sites	Vanderaveroet *et al.* (2000)
Kaolinite/chlorite	North-west Atlantic, upper slope	ODP	902D	38°56'N	72°46'W	808	Middle Eocene–Holocene	Increased chlorite supplies from north-east Atlantic during glacials	Vanderaveroet *et al.* (1999)
Clay mineralogy	Greenland margin (Labrador Sea)	90-013-013		58°12'N	48°22'W	3379	22–8 kyr	Intensification of Western Boundary Undercurrent over Late Glacial/Holocene transition	Fagel *et al.* (1999)
		91-045-094		50°12'N	45°14'W	3380	Last 18 kyr	No climate signal, dilution by detrital carbonates	
		ODP105	646	58°13'N	48°22'W	3440	Last 365 kyr	Variable provenance and deep current intensity over glacials/interglacials	Fagel & Hillaire-Marcel (2006)
Kaolinite/chlorite	Namibian margin (south-west Atlantic)	GeoB	1710 1712	23°43'S 23°25'S	11°69'W 12°80'W	2987 998	Last 400 kyr Last 400 kyr	Southwards advection of clays by deep water mass	Gingele & Schmiedl (1999)
	Walvis Ridge (south-east Atlantic)	GeoB	1214	24°69'S	07°24'W	3210	Last 400 kyr		
	Rio Grande (North-west Atlantic)	GeoB	2110 2821 2822	28°39'S 30°27'S 30°14'S	45°31'W 38°48'W 39°08'W	3008 3927 4267	Surface sediments	Minor influence of advection of kaolinite by deep water mass, variable kaolinite/chlorite ratio over glacials/interglacials	Gingele *et al.* (1999)
	South-east Atlantic	PS1225-1 PS1225-2	PS04/539 PS04/540	57°04'S	09°23'W	5408		Variable kaolinite/chlorite ratio over glacials/ interglacials, variable deep water advection	Dieckmann *et al.* (1996, 1999)
		PS1226-2	PS04/542	54°53'S	10°31'W	4033			
		PS1450-1	PS08/555	62°34'S	05°81'W	5334			
		PS1769-1	PS16/312	52°61'S	04°45'W	3269			
		PS1772-8	PS16/321	55°45'S	01°16'W	4137			

Table 2. Examples of studies using clay mineral-derived proxies from Neogene to Quaternary sedimentary records retrieved in lacustrine settings.

Clay proxy	Location	Project	Site	Latitude	Longitude	Water depth (m)	Age interval	Interpretation	Reference
Kaolinite/illite + chlorite	Quinghai-Tibet Plateau, China	Quinghai	ELJ	36°39'N	100°27'E	<25	8.1–4.6 Myr	Variable weathering conditions	Zeng *et al.* (2014)
							4.6–4.3 Myr	Chemical weathering > physical weathering	
							4.3–3.6 Myr	Physical weathering during cold climate	
							3.6–0.76 kyr	Physical weathering + tectonic uplift	
							Last 0.76 kyr	Physical weathering under cold and dry climate	
% illite, % smectite	Buguldeika Saddle, Baikal	BDP93	93-1 and 93-2	52.5°N	106.0°E	~350	Last 350 kyr	Variable weathering conditions according to climate, more smectite during interglacials, more illite during glacials	Yuretich *et al.* (1999)
							600–350 kyr	Proximal supplies to tectonic control	
Smectite composition	Buguldeika Saddle, Baikal	VER93-2	GC24	52°03'N	106°08'E	355	Last 20 kyr	Abundance of smectite layers in illite–smectite	Solotchina *et al.* (2002)
Clay mineralogy	Academician Ridge, Baikal	BDP96		53°41'N	108°21'E	330	2.5–0 Myr	Greater physical weathering under colder climate	Müller *et al.* (2000)
							Older than 3 Myr	Greater chemical weathering under warmer climate	
							5.3–2.5 Myr	More smectite during warmer interval	Sakai *et al.* (2005)
							2.5–0 Myr	More illite during colder interval	
		BDP98		53°44'N	108°24'E	333	6.7–2.7 Myr	More smectite during warmer interval	
		VER96-2-st 3		52.5°N	106.0°E	333	2.7–0 Myr Last 250 kyr	More illite during colder interval	
		VER94-st 16		53.5°N	108.0°E	310	Last 23 kyr	Variable weathering conditions according to climate	Horiuchi *et al.* (2000)
Smectite composition	Academician Ridge, Baikal	VER98-1-3		53°44'N	108°19'E	373	~250–55 kyr	Supplies of reworked smectites during glacials, more chemical weathering during interglacials	Fagel *et al.* (2003)
		VER98-1-14		53°31'N	107°58'E	412	~250–20 kyr		
Smectite/illite	Academician Ridge, Baikal	CON01-603-2a		53°57'N	108°54'E	386	Last 20 kyr	Variable weathering conditions according to climate, more smectite during interglacials + reworked smectite during glacials	Fagel & Boës (2008)
							136–114 kyr		Fagel & Mackay (2008)
	Posolsky Bank, Baikal	CON01-604-2a		52°08'N	105°86'E	133	Last 20 kyr		Fagel & Boës (2008)
Bulk mineralogy	Chew Bahir, Ethiopia	CB01		4°5'N	36°47'E	Palaeolake	Last 45 kyr	Abundance of illite during arid period	Foerster *et al.* (2012)
Clay chemistry reflection 060	Chew Bahir, Ethiopia	CB-01, CB-03, CB-05		4.1–6.3°N	36.5–38.1°E	Palaeolake	Last 20 kyr	Formation of authigenic clays during low lake level	Foerster *et al.* (2018)
Clay mineralogy	Turkana, Kenya	LT84-2P		03°08'S	36°30'E	>70	Last 10 kyr	Influence of climate and lake water chemistry	Yuretich & Ervin (2002)
	Malawi, Kenya	M86-P17		10°02'S	34°02'E	Not determined	Last 14 kyr	Reworked kaolinite	
Bulk mineralogy	Lukeino, Kenya	sedimentary outcrops		00°45'N	35°52'E	Palaeolake	6.09–5.68 Myr	Variable drainage according to climate	Dericquebourg (2016)
Bulk mineralogy	Central Mexico crater lakes	LLEs19-2		19°54'N	101°46'W	30	Last 600 yr	Variable kaolinite according to lake level	Fagel *et al.* (2024)
		LTe19-4		19°48'N	101°27'W	<9	Last 430 yr		
		LTa19-3		19°12'N	101°27'W	28	Last 160 yr	Variable kaolinite supplies and runoff with fixed lake level	

by erosion of kaolinite-rich Mesozoic sedimentary rocks and palaeosoils ('relict soils') outcropping along the Alaskan and Canadian margins (Darby, 1975). Kaolinite is formed by intense chemical weathering leading to the extensive leaching of cations and silica, occurring under warm and humid tropical-like conditions (Millot, 1970). Its presence in Arctic sediments under conditions unfavourable to its formation did not provide any climate information. In a similar way, smectite-rich layers observed in glacial sediments of Lake Baikal were interpreted as reworked clay minerals from Jurassic sedimentary rocks present in the watershed (Fagel *et al.*, 2003). The presence of smectite, which would be incompatible with cold and dry glacial conditions, pointed to a reworked clay mineral with no significance of the climate.

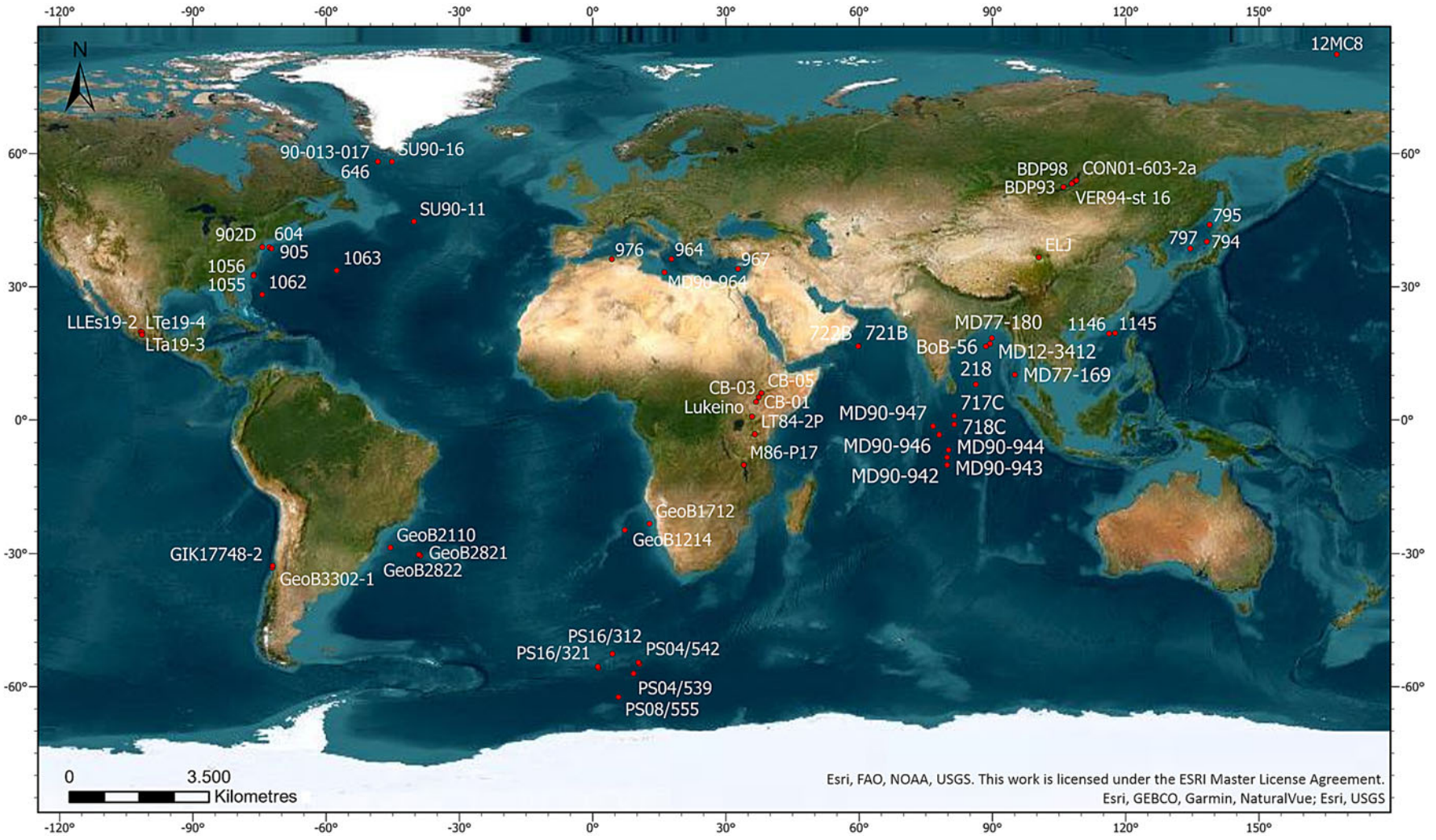

Figure 2. Examples of sedimentary cores or outcrops from marine and lacustrine settings using clay mineral assemblages as proxies for climate variability, tectonic events or provenance. More explanation and references are given in Tables 1 & 2.

Methodology

Sample preparation and analysis

X-ray diffraction (XRD) is the most common method used to identify clay minerals on oriented or random preparation (Środoń, 2003). The identification of clay minerals is usually made on the <2 µm fraction separated by gravitational settling of the bulk sediment in a column of water to reduce the influence of non-clay minerals (Brown & Brindley, 1980) The <2 µm fraction (referred as the 'fine fraction') corresponds to the granulometric definition of a clay fraction. Some pre-treatments may be applied on the bulk sample to remove carbonates, sulfates, Fe- and Al-oxyhydroxides and/or organic matter (e.g. Moore & Reynolds, 1997).

The preparation of oriented mounts from the <2 µm fraction is achieved either by sedimentation on a glass slide, centrifugation or filtration on a porcelain plate (see more details in Velde, 1992). Three diffractograms are then obtained in sequence from a sample (first: normal or air-dried; second: solvation; third: heating) to distinguish and identify the various clay minerals according to their expandability under ethylene-glycol solvation and their response to heating at 500°C (e.g. Holtzapffel, 1985).

XRD semi-quantitative approach

The abundance of the clay minerals in the clay fraction can be derived from several analytical procedures. The common method of Biscaye (1965) estimates the percentages of the clay minerals from the glycolated sample, using the area of the peak at 17 Å for smectite, 10 Å for illite and 7 Å for kaolinite and chlorite, with the proportion of kaolinite and chlorite measured according to their peak heights at 3.57 Å (002 peak of kaolinite) and 3.53 Å (004 peak of chlorite), respectively. Each peak area is calculated by multiplying the peak height by its width at mid-height. Several open-access computer programs such as *MACDIFF* (Petschick, 1997) or *HIGHSCORE* (Malvern Panalytical) perform this operation. Other methods, however, use peak heights rather than peak areas (e.g. Thorez, 1976; Holtzapffel, 1985; Boski *et al.*, 1998). In any case, all methods apply corrective factors to the measured peak area or height to take into account the intrinsic intensity of the peaks and the crystal order of the clay mineral (Holtzapffel, 1985). Such an approach is frequently semi-quantitative, providing relative abundances of clay minerals and trends of clay mineral composition between samples rather than absolute percentages. Most interpretations are indeed derived from the evolution of the clay mineral ratio rather than abundance of one clay mineral.

XRD quantitative approach

XRD on bulk powder allows for the identification of clay minerals in randomly oriented samples and the quantification of their abundance (e.g. Dietel *et al.*, 2019). Since the pioneering work of Rietveld (1967, 1969), the quantification is derived from the measurement of intensities of selected reflections and a comparison with reference intensities from internal or external reference phases (Snyder & Bish, 1989). Mineral identification is performed by comparing the peak positions and their relative intensities to diffraction data from pure phases using databases (e.g. Powder Diffraction File; ICDD, 2016; Gates-Rector & Blanton, 2019). Mineral quantification uses peak intensities, assuming that the intensities of diffraction peaks from a given phase are related to its abundance in a mixture (Chipera & Bish, 2002). Środoń (2002) stressed that the accuracy of the quantification is strongly influenced by sample preparation, data processing and selection of standards. The quantitative XRD approach requires an identical degree of orientation for all of the particles, obtained either by careful loading of the sampler holder (Środoń *et al.*, 2001) or preparation of spherical aggregates by spray drying (Hillier, 1999). Although a perfect orientation is not always guaranteed (Kaufhold *et al.*, 2012), computer-based simulation methods have been developed to quantify clay minerals from random preparations (e.g. Egli *et al.*, 2008; Casetou-Gustafson *et al.*, 2018).

The data processing of powder XRD traces can be carried out according to the reference intensity ratio (RIR) method, the full-pattern fitting method or the Rietveld refinement method. The RIR method (Bish & Chipera, 1988) is based on the measure of the diffraction intensity of a mineral phase relative to that of a standard (e.g. corundum) measured in a 50/50 (w/w) mixture (Hillier, 2000). The full-pattern fitting method (Omotoso *et al.*, 2006; Raven & Self, 2017) quantifies mineral abundance in complex mixtures by treating the diffractogram of a given mixture as the sum of contributions from individual mineral components. This approach requires calibration and collection of pure reference mineral patterns (Kaufhold *et al.*, 2012). Several computer programs (e.g. *FULLPAT* (Chipera & Bish, 2002); *RockJock* (Eberl, 2003); *powdR* package (Butler & Hillier, 2020, 2021)) combine the advantages of the RIR method with those of the full-pattern fitting method. The Rietveld method (e.g. Bergmann *et al.*, 1998; Ufer *et al.*, 2008, 2012; Dietel *et al.*, 2019) minimizes the differences between an observed XRD trace and one calculated based on crystal structure models by varying mineral composition and several other parameters (e.g. scale factor, unit-cell size, background; Chipera & Bish, 2002). Specific software using Rietveld refinement have been developed, such as *Topas* (Bruker) or *Profex* (open source). However, the application of the Rietveld approach requires knowledge of the crystal structures of all mineral components present in the samples (Chipera & Bish, 2002). Since 2002, significant improvements in analytical techniques for the quantification of clay-bearing complex mixtures have been stimulated by the biannual round-robin competition called the Reynold's Cup (e.g. McCarty, 2002; Omotoso *et al.*, 2006; Raven & Shelf, 2017; Butler & Hillier, 2021).

Studies from marine sediments

Since 1968, Deep-Sea Drilling Projects (DSDP; 1968–1983), Ocean Drilling Projects (ODP; 1983–2007) and International Ocean Drilling Projects (IODP; until 2004) have improved our understanding of the provenance and transport pathways of marine sediments. The evolution of clay mineral assemblages through core-depth analysis was investigated in many oceanic basins to reconstruct either changes of weathering conditions in the adjacent continental watershed or of atmospheric/oceanic current pathways (Fig. 2 & Table 1).

Arabian Sea: identification of sediment sources, means of transport and climatic controls

Site description

In the Arabian Sea (north-western Indian Ocean; Fig. 3), the climate is controlled by the monsoon regime (Kutzbach, 1981; Prell, 1984). The monsoon phenomenon corresponds to a seasonal reversal of wind direction. Driven by the land–sea thermal

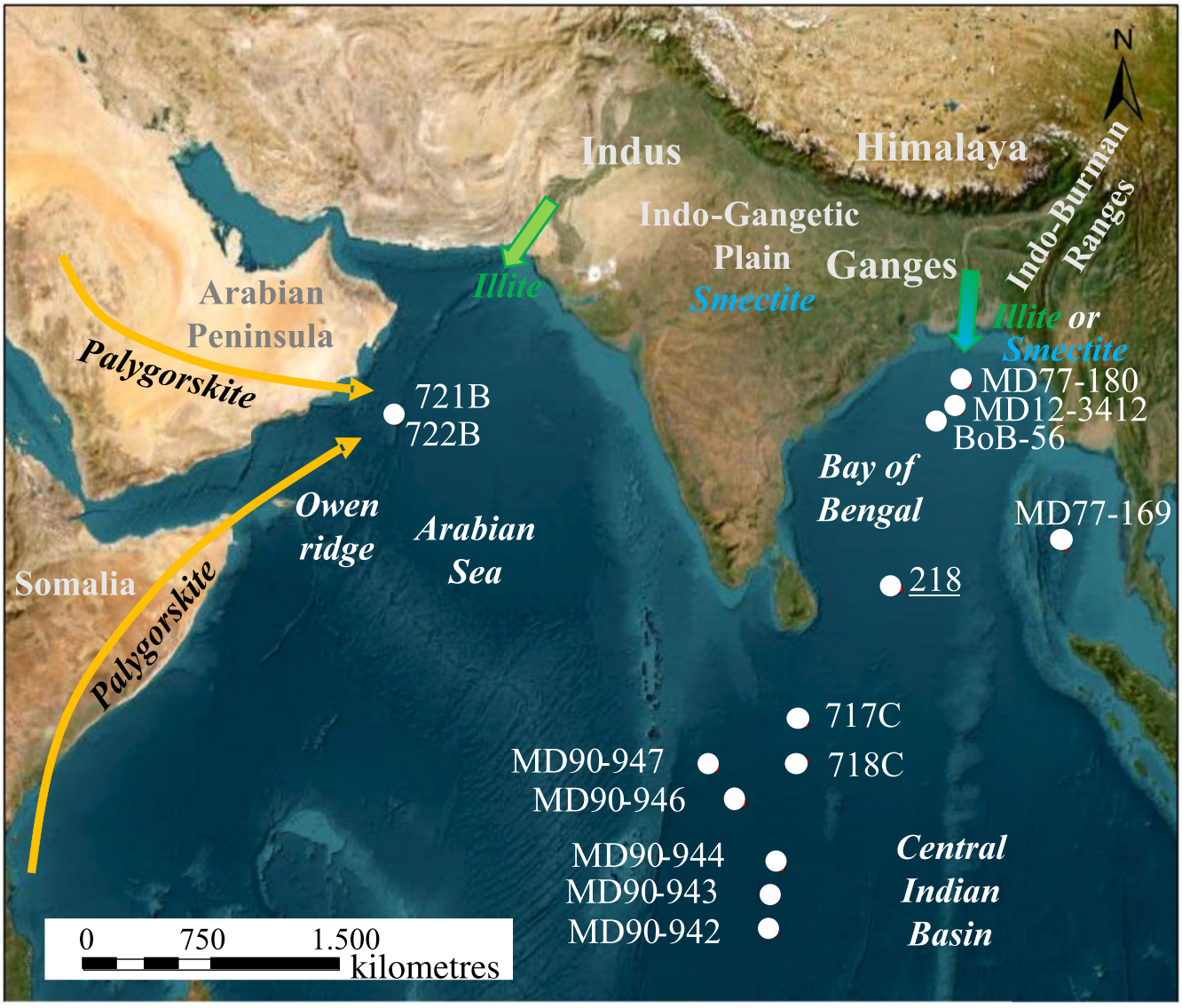

Figure 3. Location of coring sites in the Arabian Sea, Bay of Bengal and Central Indian Basin in the Indian Ocean, including DSDP (underlined number), ODP (plain number) and Marion Dufresne (MD) drilling campaigns. The arrows represent the main transport of clay minerals to the adjacent basins. The orange arrows indicate the south-western summer monsoon and associated north-western trade winds that transport palygorskite-rich dust to the Owen Ridge. Illite (and chlorite to a lesser extent) is delivered by fluviatile transport (Indus or Ganges). Smectite, mainly originating from the Indo-Gangetic Plain, is delivered by fluviatile transport to the Bay of Bengal and Central Indian Basin.

contrast, monsoons affect the annual weather cycle between 30°N and 30°S. The south-west summer monsoon provides strong and wet winds, whereas the north-east winter monsoon brings weak and dry winds. The Owen Ridge is a key site in the north-west Indian Ocean for observing the onset and behaviour of the monsoonal circulation pattern using clay proxies. Indeed, the site is characterized by two contrasting sources in terms of clay mineralogy. During the summer monsoon, the south-westerly winds sweep the saline desert area of Somalia along the East African coast and Arabian Peninsula, bringing significant amounts of palygorskite (Debrabant *et al.*, 1991; Krissek & Clemens, 1991). Nair *et al.* (1989) estimated that during the summer 80% of detrital fluxes were delivered to the Owen Ridge by the south-western monsoon winds. In winter, the north-east monsoon is weak. However, south-central Asia still receives rainfall draining the Himalayan highlands. Illite released by physical erosion from the Himalayas is transported by the Indus River towards the Owen Ridge (Fagel *et al.*, 1992b). Since the Middle Miocene, the ridge was uplifted above the level of active Indus-derived turbiditic flows (Debrabant *et al.*, 1991). Following the uplift, the clay minerals are delivered to the Owen Ridge mainly by aeolian transport (from the west and south) and oceanic currents (from the north). The continuous hemipelagic sedimentation (35 m/Myr) on the Owen Ridge was expected to record a climatic influence that was masked in the adjacent deep-sea fans.

Materials and methods

The coring site 721B (16°40.636'N, 59°51.879'E; Fig. 3) recovered 450 m of early Miocene to Pleistocene sediments (Debrabant *et al.*, 1991). Analysis of the fine fraction was conducted on the Pliocene–Pleistocene sedimentary interval in the upper unit 1A of Site 721B (Leg ODP 117; Debrabant *et al.*, 1991), between

2.7 and 1.2 Myr, totalling 300 samples (Fagel *et al.*, 1992b). The sediments of unit 1A were composed of nanofossil oozes.

XRD analysis was carried out on oriented mounts after decarbonation and settling to retrieve the <2 µm fraction. The measurements were performed at the University of Lille I (France) using a Philips PW 1730 diffractometer equipped with a copper anticathode. The semi-quantification of the clay minerals (±5%) was conducted according to the method proposed by Holtzapffel (1985), using diagnostic peak heights multiplied by corrective factors. Peak height ratios were measured on the XRD trace of glycolated mounts as a clay mineral proxy. The chosen proxy P/I (i.e. palygorskite/illite ratio) corresponds to the ratio between the 10.4 Å peak of palygorskite and the 10.0 Å peak of illite. Over the studied interval, the P/I ratio ranged between 0.35 and 1.20 with a standard deviation of 0.03–0.05 measured using 3 samples and 10 preparations of each (Fagel *et al.*, 1992b). The P/I ratio values were reported as a function of time. A constant sedimentation rate was assumed, which allows us to define a time series (Li *et al.*, 2018; Meyers, 2015) that may be further treated by spectral analysis (Fig. 4). This statistical approach is based on various mathematical transformations (e.g. discrete Fourier transform [DFT], discrete Fourier transform on the autocorrelation [DFTA]; Press *et al.*, 1986; Beaufort, 1996) that are applied to the time series to reveal any periodicity (Jenkins & Watts, 1968). The results of DFT and DFTA give the intensity of the signal (*y*-axis) as a function of a spectral index (*n*, *x*-axis). In such diagrams, each peak corresponds to a period (T_x) obtained by dividing the duration of the studied interval (I) by the spectral index (x; i.e. $I/x = T_x$).

Earth's climate is influenced by periodic changes in Earth's orbital parameters (Hays *et al.*, 1976; Berger, 2012). These so-called Milankovitch cycles include precession (~20 kyr), obliquity (41 kyr) and eccentricity (~100 kyr, in turn modulated by a 405 kyr cycle; Fig. 4; Laskar *et al.*, 2011). Palaeoclimate proxies are used to detect orbital forcing in sedimentary series and to establish accurate orbital timescales, notably for the Cenozoic (Lourens *et al.*, 2005).

Results and interpretation

The studied clay mineral assemblage of core 721B consisted of palygorskite (20–50%), smectite (20–45%), illite and irregular illite–smectite mixed-layer 10–14 (10–30%), chlorite (5–20%) and kaolinite (0–10%). The clay mineralogy displayed a marked negative correlation between the relative abundances of palygorskite and illite over core depth. The average coefficient of correlation between palygorskite and illite was –0.61, although it varied with the age of the sediment (Fagel *et al.*, 1992b). Accordingly, palygorskite and illite have different sources, so that fluctuations in clay mineral assemblages most probably reflect repeated inversions of atmospheric circulation related to the Indian monsoon. Palygorskite-rich intervals indicate intense aeolian supplies by the strong summer monsoon, whereas illite-rich intervals record fluviatile supplies by the Indus during the weak winter monsoon (Fig. 3).

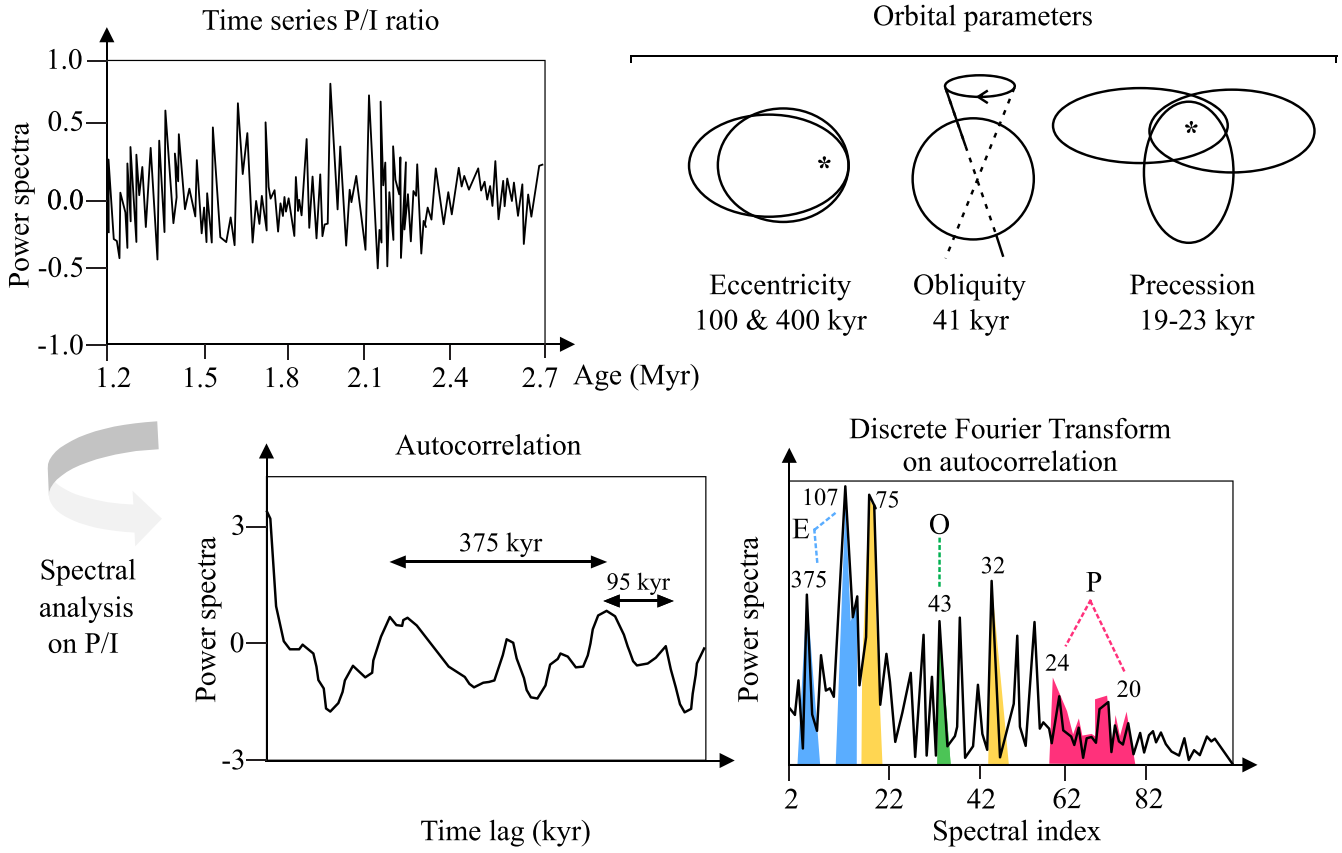

Figure 4. Spectral analysis of the palygorskite/illite (P/I) ratio over a 1.5 Myr interval between 2.7 and 1.2 Myr in core 721B retrieved from Owen Ridge (top left, modified from Fagel *et al.*, 1992b). Top right: orbital parameters that modify climate and related events. The lower graphs represent the results of spectral analysis. In the autocorrelation, the period of 95 kyr indicates control by the eccentricity of Earth's orbit. The DFTA demonstrates orbital control by the three orbital parameters (E = eccentricity in blue; O = obliquity in green; P = precession in red). The periods observed at 32 and 75 kyr probably correspond to non-linear combinations between various orbital parameters.

A spectral analysis was performed on the evolution of the P/I ratio between 2.7 and 1.2 Myr to reveal any periodicity in the time series. The result of autocorrelation on the 1.5 Myr-long interval revealed two periods of 95 kyr and of 375 kyr (Fig. 4). Such periods are within the range of the characteristic periods of the eccentricity of Earth's orbit (Fig. 4). Although the spectral analysis revealed numerous peaks, it is only possible to interpret those peaks for which a cause can be established (i.e. those that are probably linked to the three orbital parameters; Berger, 1977). In the DFTA, the period of 107 kyr ($n = 14$) most probably reflects the influence of the eccentricity on clay sedimentation on the Owen Ridge. The period of 43 kyr ($n = 35$) probably records the influence of the obliquity, whereas the periods comprising between 24 and 20 kyr ($62 < n < 75$) demonstrate the influence of precession on clay sedimentation. A period of 375 kyr ($n = 4$) is also observed in the autocorrelation, but the time series is too short to confirm it. The intense peaks observed at 75 and 32 kyr in the DFTA probably correspond to non-linear combination of the orbital parameters (Ruddiman & McIntyre, 1981; Clemens & Prell, 1991).

In addition, the spectral analysis of the range between 2.7 and 1.2 Myr was performed on successively shorter intervals of 375 kyr to investigate any evolution of the main orbital control through time. Figure 5 compares the results of the autocorrelation and the DFTA analyses on two successive intervals. The oldest interval, between 2.7 and 2.3 Myr (Fig. 5a), presents a strong periodicity between 19 ($n = 20$) and 23 kyr ($n = 16$), indicating a dominant precession influence, confirmed by the periodicity of 21 kyr observed in the autocorrelation (Fig. 5a, inset). For the next interval (2.3–2.0 Myr; Fig. 5b), the highest intensity detected in DFTA coincides with a period of 42 kyr ($n = 9$), indicating control by obliquity, as was also confirmed by the results of autocorrelation (Fig. 5b, inset). The same result was obtained from the magnetic susceptibility profile of core 721B (De Menocal *et al.*, 1991). The transition from predominant control by precession to obliquity occurs at 2.4–2.3 Myr, within a time interval corresponding to the extension of the Northern Hemisphere glaciations (Shackleton *et al.*, 1984). Supporting this interpretation, De Menocal *et al.* (1991) proposed that the Indian monsoon, at low latitude, was slightly affected by the expansion of the ice sheets in the high latitudes of the Northern Hemisphere. In summary, the variability observed in the Neogene clay sedimentation on the Owen Ridge is strongly controlled by climate, with different sources involved over seasons and linked to the Indian monsoon.

Bengal Fan, northern Indian Ocean: fluviatile transport and weathering conditions

Site description

Proximal environments on the ocean floor such as fans and deltas have been widely studied to trace the origins of detrital supplies. The clay assemblages of those proximal environments are under the direct control of the adjacent continental landmasses. For instance, the Bengal Fan (Fig. 3), the largest submarine fan in the world (Curray *et al.*, 2003), receives both the physical weathering products of Himalayan highlands (i.e. primary minerals illite and chlorite) and the chemical weathering products of the Indo-Gangetic Plain soils (i.e. secondary minerals, mainly smectite; Srivastava *et al.*, 1998) *via* fluviatile transport by the Ganges and Brahmaputra rivers (Venkatarathnam & Biscaye, 1973; Kolla & Rao, 1990). Since the Bengal Fan sediments are very sensitive to monsoon rainfall, this study allows us to determine the relationships between regional climate and continental erosion (e.g. Joussain *et al.*, 2016).

Clay mineral variability was investigated in several marine cores at both proximal (e.g. MD77-180 (Colin *et al.*, 1999); BoB-56 (Li *et al.*, 2018)) and distal Bengal Fan sites (e.g. DSDP 218 (Bouquillon *et al.*, 1989); ODP Leg 116 Site 717C (Bouquillon *et al.*, 1990; Brass & Raman, 1990; Aoki *et al.*, 1991); Fig. 3). In the <2 μm fraction, the clay mineral assemblages are characterized by changes in the relative abundance of illite and smectite over long timescales, from the early Miocene to Pleistocene. This mineral variability is explained either by changes in relative sedimentary inputs from Himalayan and Indian sources and/or changes in weathering intensity in the Indo-Gangetic Plain (e.g. Bouquillon *et al.*, 1990; Aoki *et al.*, 1991; France-Lanord *et al.*, 1993; Derry & France-Lanord, 1996).

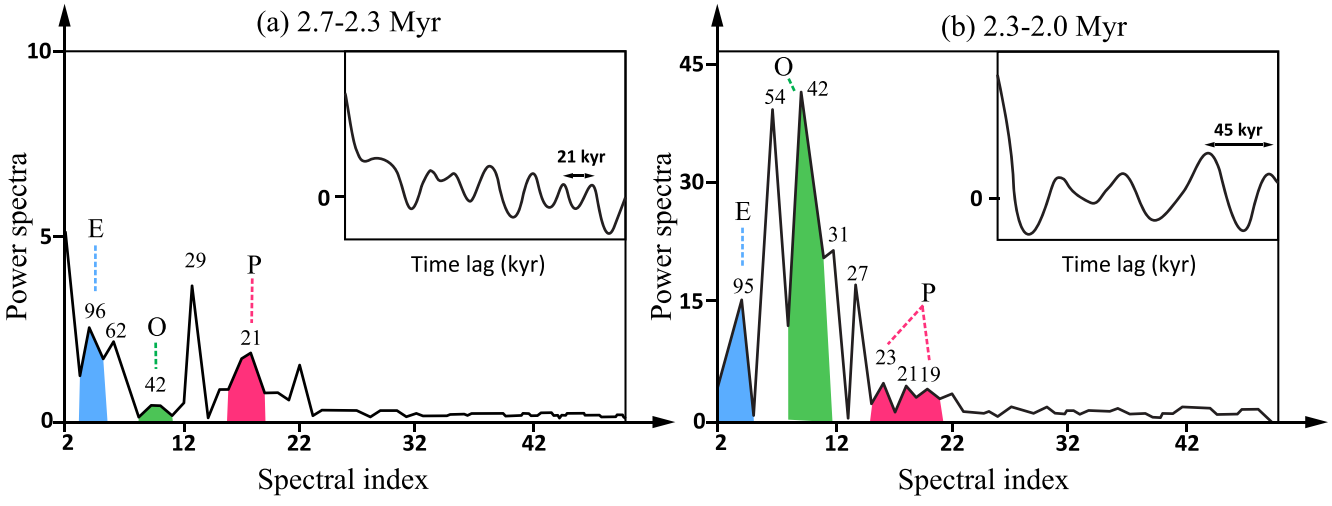

Figure 5. Spectral analysis of the palygorskite/illite (P/I) ratio at two successive intervals of 375 kyr between 2.7 and 2.0 Myr of core 721B retrieved from Owen Ridge (modified from Fagel *et al.*, 1992b). Large graphs: The dominant periods obtained by DFTA for (a) 2.7–2.3 Myr and (b) 2.3–2.0 Myr. For the colour code, see Fig. 4. The oldest interval (2.7–2.3 Myr) is marked by dominant precession (P) control that evolves towards obliquity (O) control between 2.3 and 2.0 Myr. The insets represent the autocorrelation function. In these graphs, the distance between two peaks indicates the type of orbital control. E = eccentricity.

Materials and methods

Joussain *et al.* (2016) analysed the clay mineral assemblages in core MD12-3412 over the last 180 kyr with a millennial resolution. The 32 m-long core MD12-3412 (17°10'94"N, 89°28'92"E) was retrieved in the upper part of the Bengal Fan at a water depth of 2368 m near the continental slope (north-eastern Bay of Bengal; Fig. 3). Its hemipelagic sediments consisted of intercalations of clayey and silty layers interrupted by gravity-flow depositions (i.e. turbidites) related to changes in the regime of Ganges discharges. The $\delta^{18}O$ *vs* depth curve from planktonic foraminifera, combined with seven radiocarbon ages, was correlated with the reference marine oxygen isotope composition *vs* time curve SPECMAP (Martinson *et al.*, 1987) to establish an age model for core MD12-3412, which produced an estimate of a high sedimentation rate ranging between 3 and 11 cm kyr^{-1}.

Only the upper 13.5 m of core MD12-3412 (i.e. ~180 kyr) was sampled at 5–10 cm intervals for clay mineralogical analyses ($n = 240$). Oriented mounts of carbonate-free <2 µm fractions were investigated using XRD (Holtzapffel, 1985). The analysis was performed using a PANalytical X'Pert Pro Diffractometer equipped with a copper anticathode (Cu-*K*α) and a Ni filter, under a voltage of 40 kV and a current intensity of 25 mA. The samples were measured with a counting time of 1 s/step in the range 3–30°2θ. The relative abundance of the main clay minerals was derived from the measurement of peak areas of the basal reflection (10 Å for illite, 7 Å for chlorite and kaolinite, 15–17 Å for smectite) on glycolated mounts using *MacDiff* software (Petschick, 1997). The relative proportions of kaolinite and chlorite were estimated using the (002) peak of kaolinite and the (004) peak of chlorite (i.e. 3.57 Å/3.54 Å; Biscaye, 1965).

Results and interpretation

According to the age model, the upper 13.5 m of core MD12-3412 covered Marine Isotopic Stages (MISs) 6 to 1 (Martinson *et al.*, 1987), encompassing several glacial (MISs 6 and 2) and interglacial (MISs 5 and 1) periods. Over the studied interval, smectite (11–64%) and illite (18–49%) were the predominant clay minerals, followed by chlorite (10–39%) and kaolinite (5–12%). The fluctuations of smectite over glacial and interglacial periods were negatively correlated with illite and chlorite variations. The upper sediments of core MD12-3142 were expressed as [Sm/I + C], the clay mineral abundance ratio between smectites and the sum of illite and chlorite. The ratio [Sm/I + C] is a proxy for weathering conditions in the adjacent continental area. More physical erosion during glacial periods leads to an enrichment of primary minerals, illite and chlorite and a low [Sm/I + C]. By contrast, warmer interglacial intervals enhance chemical weathering with more production of secondary clays, mainly smectite, in the soils of the Indo-Gangetic Plain, resulting in high [Sm/I + C] values. On average, the [Sm/I + C] ratio is <0.5 during glacial periods, whereas it reaches up to 1 and, more rarely, 2 in interglacial intervals. Therefore, interglacial periods were marked by a significant increase in the proportion of smectite (high [Sm/I + C] ratios), whereas glacial periods were characterized by an increase in illite and chlorite (low [Sm/I + C] ratios). In particular, Joussain *et al.* (2016) explained the observed [Sm/I + C] maxima during interglacial MIS 5 either by an intensification of summer monsoon rainfall or by a reinforced summer surface oceanic current, both processes leading to greater delivery of smectite to the Bay of Bengal.

The glacial–interglacial variations also had an influence on sea level. During the higher sea level of the last interglacial, turbidity currents were focused on the active submarine channel located in the eastern part of the Bay of Bengal (Weber *et al.*, 1997; Curray *et al.*, 2003), leading to greater proportions of detrital material from the Ganges–Brahmaputra river system in core MD12-3412 (Fig. 3). During glacial periods, the rivers were confined to the main channels in response of the lower sea level, resulting in more efficient delivery of detrital minerals from the Indo-Burman ranges (Fig. 3) to the north-eastern Bengal Fan.

Central Indian Basin, Indian Ocean: fluviatile transport and weathering conditions

Site description

Major tectonic, climatic and oceanic current changes have occurred in the Indian Ocean since the early Cenozoic in relation to the Alpine orogenesis (e.g. Kennett, 1982). Such changes were expected to be recorded in the Indian Ocean sediments.

Materials and methods

Five long cores (i.e. MD90-947 to MD90-942, 33–49 m long) were recovered along a north–south (1–10°S) transect at ~80°E in the Central Indian Basin (Fig. 3) during the MD90/SHIVA cruise (Fagel *et al.*, 1994). Two main lithologies were observed: a lower sedimentary unit made of reduced silty to sandy mud and an upper unit composed of oxidized siliceous clayey mud. According to radiolarian-derived biostratigraphy, the age of the sediments ranged from the Late Miocene to the Late Pliocene (<3.5/3.7 to >6.3 Myr).

The clay mineralogy was studied by XRD of the <2 µm carbonate-free fraction (Holtzapffel, 1985), with a sampling interval of 30–40 cm (i.e. ~600 samples). A Philips PW 1730 diffractometer equipped with a copper anticathode and Ni filter was used with a voltage of 40 kV and an intensity of 25 mA. Analytical uncertainties are estimated as ±5% for clay mineral abundances >20% (Holtzapffel, 1985).

In addition, the clay mineral variability was studied at high resolution in the cores MD90-946 (3°S) and MD90-943 (8°S) over three biostratigraphy-constrained intervals: specifically, between 5.7/5.8 and 6.3/6.5 Myr (Late Miocene) and between 1.2/1.5 and 4.3/4.7 Myr (Late Pliocene) for MD90-946 and between 5.0 and 5.6 Myr (Early Pliocene) for MD90-943. A total of 400 supplementary samples were analyzed by XRD to reach a resolution of 1 sample per 10 cm. The chosen clay proxy was the smectite/illite peak height ratio (S/I), which was measured on the glycolated diffractograms (Fagel *et al.*, 1994). The fluctuations of S/I ratios through core depth were reported as a function of time by applying a mass accumulation rate estimated from stratigraphic information. Then, the time series were further studied by spectral analysis to detect any periodicity in the clay mineralogy.

Results and interpretation

The clay mineralogy of the southern sites (MD90-942, MD90-943 and MD90-944; Fig. 3) is dominated by smectite (35–90%) associated with illite (5–45%), kaolinite (5–25%), chlorite (0–10%) and irregular mixed-layer minerals (0–10%). Illite (5–35%) and chlorite (0–15%) are more abundant in northern sites (MD90-946 and MD90-947; Fig. 3) than in the southern ones (3% < illite < 22%, chlorite <10%). The main supplies of illite, chlorite and irregular mixed-layer minerals were attributed to the physical erosion of the Himalayan reliefs and their river drainage systems (Nath *et al.*, 1989). In the marine environment, illite and chlorite settled rapidly due to their coarser size, whereas

smectite travelled further south, leading to an enrichment of smectite in the distal environment (differential settling process; Debrabant *et al.*, 1993).

The clay variability, expressed by the S/I ratio, was further studied at higher resolution on three intervals of cores MD90-946 and MD90-943 (Fagel *et al.*, 1994). Only the periodical cycles that were revealed in several independent mathematical functions (autocorrelation, DFT and DFTA) were considered as significant (Blackman-Tuckey, 1958). The most prominent periodical cycle was of 100 kyr (i.e. eccentricity; Fig. 4) observed in the S/I fluctuations over the Late Miocene interval (5.7/5.8 to 6.3/6.5 Myr) in core MD90-946. Therefore, Late Miocene smectite/illite variations are controlled by a periodic Earth orbital control linked to its eccentricity (Fagel *et al.*, 1994). The spectral analysis on the Early Pliocene interval (5.0–5.6 Myr) of core MD90-943 also showed control of a 100 kyr cycle in the different spectral treatments (Fagel *et al.*, 1994).

By contrast, no cyclicity was observed in spectral analysis over the Late Pliocene interval (1.2/1.5 to 4.3/4.7 Myr), suggesting non-periodic, most probably tectonic-related control over the S/I ratios in the upper part of the MD90-946 core (Fagel *et al.*, 1994). The Central Indian Basin, located in a north–south compressive stress regime, has been affected by intraplate deformation (Stein & Okal, 1978) since the late Miocene. Seismic instabilities on the Chaggos–Laccadive Ridge located at the western side of the MD90-946 core could favour some turbiditic supplies. Tectonic rejuvenation most probably explains the absence of periodic control of the sedimentation.

South China Sea, Pacific Ocean: provenance of detrital fluxes and interaction between monsoon winds and surface current transport

Site description

The South China Sea (SCS; Fig. 6) is the largest marginal sea in the Pacific Ocean. Its sedimentation reflects the complex interactions between surface oceanic current patterns, East Asian monsoon winds and subsurface and deep currents from the adjacent Pacific Ocean intruding from the south (Wang *et al.*, 2003). The East Asian monsoon, a major component of the global climate system, results from differential heating of the Asian continent and the western Pacific Ocean, which causes large seasonal contrasts in wind, precipitation and surface currents (Webster, 1987). In the summer, heating of the Asian continent generates a low-atmospheric pressure cell over central China, which induces wind to blow from south-west to north-east, bringing heavy

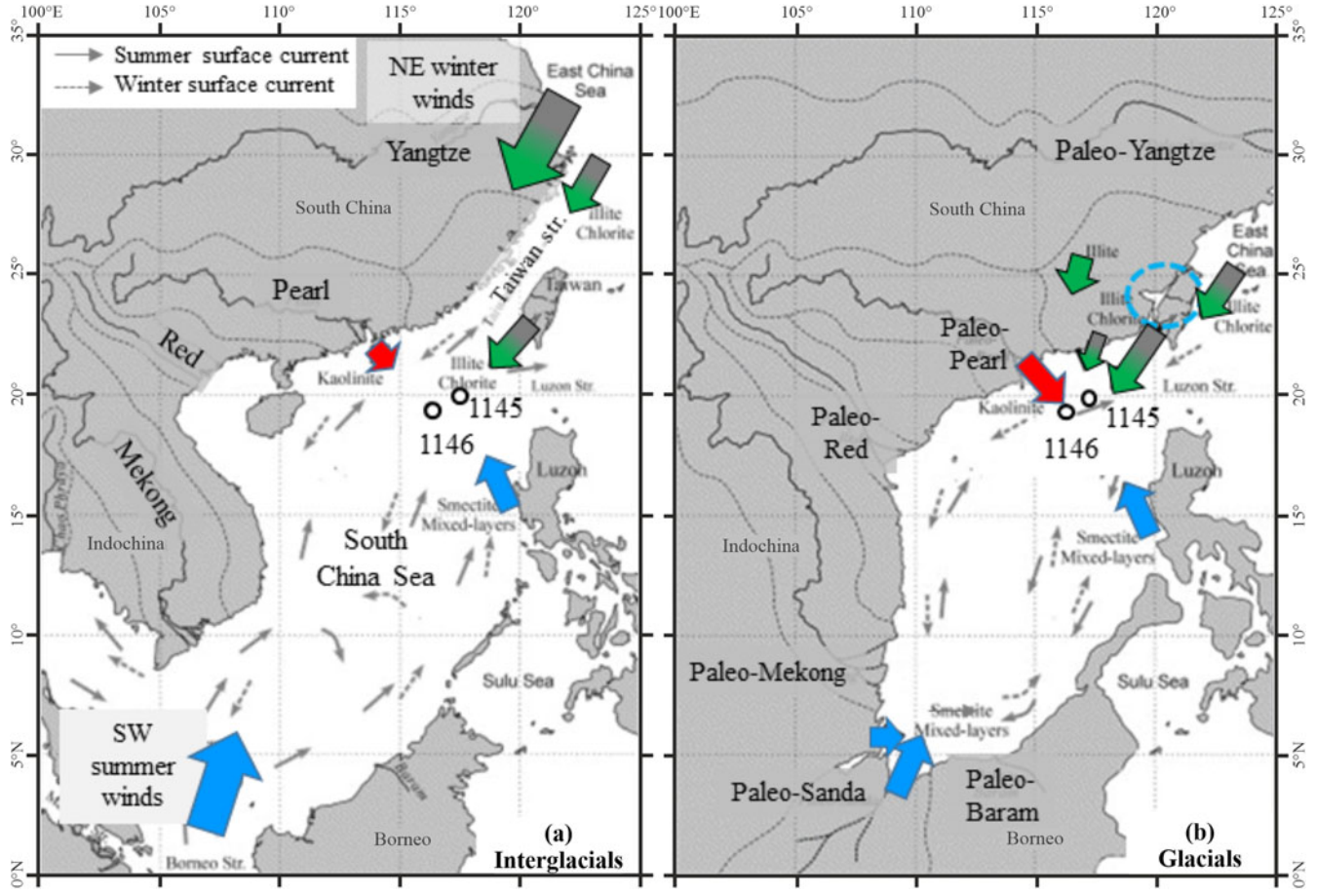

Figure 6. Location of ODP coring sites 1145 and 1146 in the SCS (modified from Liu *et al.*, 2003). The small coloured arrows indicate the provenance of clay minerals, with smectite-rich supplies in blue, illite in green, chlorite in grey and kaolinite in red. The lengths of the arrows indicate the relative importance of the clay mineral contributions from the various sources. (a) Main sources of clay minerals during interglacial periods. The winter north-eastern winds mainly brought illite and chlorite that were delivered by the Yangtze River (large green–grey arrow). The summer south-western winds transport smectite produced by weathering of volcanic material (large blue arrow). The surface oceanic currents then distribute the clay minerals across the SCS (black arrows). (b) Modifications occurring during glacial periods when the SCS became a semi-enclosed basin.

monsoon rainfall over the south-eastern Asian continent (Webster, 1987). Conversely, in winter, a high-pressure cell over northern Asia related to the low temperatures over the Asian continent is responsible for dry and cold winds blowing from continental Asia to SCS in the south-west direction (Fig. 6a). In addition to local monsoon-related climatic changes, the SCS also records global glacial/interglacial oscillations (Boulay *et al.*, 2005). During glacial period, the SCS became a semi-enclosed marginal sea due to the significant sea-level drop (≥100 m; Fig. 6b). The modified glacial coastline was characterized by a clockwise surface circulation gyre in the summer and an anticlockwise gyre in the winter (Wang & Wang, 1990).

The delivery of clay minerals in the surface sediments of the SCS (Fig. 6) was controlled by the river discharge of weathering products from the adjacent Asian continent (Chen, 1978). Approximately 570 Mt yr^{-1} of suspended sediment (2.8% of global discharge to the world oceans; Milliman & Syvitski, 1992) are delivered to the SCS from three main sources (the Mekong River, the Pearl River and the Red River) and small rivers in south-western Taiwan (Liu *et al.*, 2010). The north-eastern SCS receives 46% of this discharge (260 Mt yr^{-1}) from the Pearl River, south-western Taiwan and the Luzon arc system (Liu *et al.*, 2010).

The distribution of clay minerals at the surface sediments of the SCS is mainly controlled by mineral provenance, with six mineralogical provinces being differentiated (Chen, 1978):

(1) Illite and chlorite are the dominant minerals in the northern shelf of the SCS, the Taiwan Strait and the East China Sea. They are delivered by deep-water currents to the northern SCS by mountainous rivers draining the island of Taiwan and by the Yangtze River through the Taiwan Strait, with minor aeolian contributions from northern Asia due to north-eastern winter monsoon winds.
(2) Smectite and kaolinite are somewhat greater in content (~7%) relative to illite and chlorite in the central part of the SCS and north-east Luzon Strait.
(3) Smectite is >20% around the volcanic arc of the island of Luzon. Smectite-rich supplies are further transported to the northern SCS by surface currents influenced by the Kuroshio current originating from the adjacent Pacific Ocean.
(4) Smectite reaches ~30% in the southern SCS along Malaysia and Borneo. They are supplied by the south-western summer monsoon winds and transported by the surface oceanic currents to the northern end of the SCS and to the East China Sea through the Taiwan Strait (Fig. 6a; Liu *et al.*, 2003, 2010).
(5) Kaolinite represents 50% of the clay mineral assemblage in the estuary of the Pearl River, then decreases downslope, probably due to rapid settling of coarse particles.
(6) Illite and chlorite are abundant in the estuary of the Mekong River (47% and 23%, respectively).

The relative contributions of clay minerals in the SCS sedimentary record were affected by the modified morphology of the SCS during glacial periods due to a sea-level drop of ~100 m (Fig. 6b). The SCS became a semi-enclosed basin characterized by an anticlockwise surface circulation driven by the winter monsoon winds (Wang *et al.*, 1995). More supplies of kaolinite were delivered to the coring site by the Palaeo-Pearl River due to the significant south-eastern shift of its estuary. Illite was mainly supplied from the island of Taiwan, whereas smectite was delivered to the south SCS by the Palaeo-Sanda River and to the north-eastern SCS from the island of Luzon. The distribution of clay minerals in SCS sediments may be used to trace the provenance and to identify the main transport agents supplying the detrital clay minerals to the marginal oceanic basins (Lui *et al.*, 2003, 2010).

Materials and methods

ODP site 1146 (19°27.40'N, 116°16.37'E) was drilled on the continental slope of the northern SCS, at a water depth of 2092 m and near to the Pearl River estuary (Fig. 6). The sediments consisted of nannofossil-containing clays. The samples ($n = 515$) were retrieved from the upper 190 m of holes 1146A, B and C. The oxygen isotope record measured using foraminifera *Globigerinoides ruber* (surface-dwelling planktonic species) of ODP Site 1146 was correlated to the reference $\delta^{18}O$ curve of ODP Site 677 in the east Atlantic (1°12'N, 83°44'W, 3461 m water depth; Shackleton *et al.*, 1990). The studied interval covered the last 2 Myr. According to the age-depth model, derived from a combination of oxygen isotope stratigraphy, biostratigraphy and palaeomagnetism, the sampling interval of ~40 cm provided an average temporal resolution of 4 kyr (Liu *et al.*, 2003).

Clay minerals were identified by XRD on oriented mounts of carbonate-free, clay-sized particles (<2 μm) according to the methodology of Holtzapffel (1985). The analysis was performed using a Philips PW 1710 diffractometer with Cu-*K*α radiation and Ni filter, with a voltage of 40 kV and a current intensity of 25 mA (Trentesaux *et al.*, 2003). Three analyses were performed per sample for air-dried and glycolated conditions in the 2.5–32.5°2θ range and from 2.5 to 14.5°2θ for heated samples (2 h at 490°C). Semi-quantitative estimates were derived from measurements of the glycolated mounts using the peak areas of the following peaks: smectite at 17 Å, mixed-layer illite–smectite at 15 Å, illite at 10 Å and kaolinite/chlorite at 7 Å, using the *MacDiff* software (Petschick, 1997). The clay mineral ratio (smectite + illite–smectite)/(illite + chlorite) was calculated from the peak areas to evaluate the controls over clay mineral variations over the last 2 Myr (Liu *et al.*, 2003). A spectral analysis was performed on the evolution of the clay mineral ratio (smectite + illite–smectite)/(illite + chlorite) to reveal any periodicity in the time series covering the last 2 Myr.

Results and interpretation

The clay minerals in ODP site 1146 (Fig. 6) are dominated by illite (22–43%) and smectite (12–48%), associated with chlorite (10–30%), kaolinite (2–18%) and illite–smectite and chlorite–smectite (5–22%; Liu *et al.*, 2003; Trentesaux *et al.*, 2003). Over the last 2 Myr, the clay mineral assemblages display opposing trends for (illite + chlorite) and smectite. Illite and chlorite display similar variations, with higher values during glacial intervals (35% < illite < 43%, 20% < chlorite < 30%; Liu *et al.*, 2003). Higher values of smectite (>30%) occur during interglacial periods. Kaolinite averages 12%, with greater values occurring during glacials. Because the irregular mixed-layer minerals evolve in parallel with smectite, both minerals were merged into 'smectite'. The clay variability was represented by the evolution of the ratio smectite/(illite + chlorite) over the last 2 Myr (Liu *et al.*, 2003). The ratio [S/(I + C)] displays a range of variation between 0.3 and 1.8 (average value 0.9), with higher [S/(I + C)] ratios systematically reported during interglacials. This variation is correlated with the oxygen isotope record, particularly before 1 Myr. The correlation is moderate from 1000 to 400 kyr then poor in the upper 400 kyr of the record. Because this [(S/(I + C)] ratio was shown to be related to climatic conditions, it was chosen as a proxy for East Asian monsoon variability (Liu *et al.*, 2003). A lower ratio indicates a stronger winter monsoon during

glacials, whereas a higher ratio indicates stronger summer monsoon winds during interglacials. Such clay mineral variability over glacial/interglacial periods is related to the provenance of clay minerals and their transport by surface marine currents and seasonal monsoon winds through the SCS (Liu *et al.*, 2010).

Spectral analysis of the chosen clay mineral ratio at ODP Site 1146 revealed a strong peak at 41 kyr, suggesting a dominant orbital control by obliquity over the past 1.8 Myr (Liu *et al.*, 2003). Among the orbital parameters, obliquity exerts its main influence at low latitudes (Nesje & Dahl, 2000), with a significant influence on the monsoon. However, the three orbital parameters play a role in the strength of the seasonal monsoon system (Lupien *et al.*, 2023): precession influences the monsoon strength over 21 kyr cycles by modulating the pressure and temperature contrasts between oceans and continents; eccentricity modulates the amplitude of precession variability at a given latitude; and obliquity controls the latitudinal and seasonal distribution of insolation.

In addition to the analysis of the whole interval, Liu *et al.* (2003) also performed a spectral analysis on 10 successive 200 kyr-long intervals to determine whether there had been any evolution of the main orbital control over time (Liu *et al.*, 2003). The results revealed the strongest obliquity influence in the interval between 1.6 and 1.2 Myr, suggesting a major influence of monsoon-related transport processes. Between 1.2 and 0.6 Myr, two periods at 41 and 100 kyr were observed. Their common occurrence probably recorded the combined influence of monsoon (controlled by 41 kyr cycles) and glacial/interglacial sea-level changes (controlled by 100 kyr cycles). For the last 600 kyr, there was a peak at 100 kyr, suggesting a main contribution of glacial/interglacial sea-level changes in the clay variability. In summary, Liu *et al.* (2003) found a change in the main orbital control affecting the clay mineral assemblage, with a major shift at 1.2 Myr attributed to the extension of the glaciations in the Northern Hemisphere. However, it is important to remember that the resolution that can be reached in this analysis depends on the length of the time series (Martinez *et al.*, 2012). In practice, at least 5–10 repetitions along the studied time series are required to interpret a period with confidence (Weedon, 2003). Here, the studied intervals are quite short (200 kyr) relative to the revealed periodicity, especially for eccentricity (100 kyr) and, to a lesser extent, for obliquity (41 kyr; Fig. 4).

A similar approach but with a higher temporal resolution (1 kyr) was conducted on the clay mineral record of the nearby ODP Site 1145 (location on Fig. 6; Boulay *et al.*, 2005). The [S/(I + C)] ratio displayed a similar range of variation (0.30–1.55) to that for ODP Site 1146 (Liu *et al.*, 2003). A major influence of precession was shown by Blackman–Tukey spectral analysis. Precession is a major forcing factor of the summer monsoon intensity (Prell & Van Campo, 1986; Prell & Kutzbach, 1987), as observed in the Indian Ocean (e.g. in the Arabian Sea (Clemens *et al.*, 1991) or the Andaman Sea (Colin *et al.*, 1999)). Moreover, a strong relationship was found between the clay mineralogy and the solar insolation curve calculated at a latitude of 20°N (Boulay *et al.*, 2005). Each maximum of the insolation curve corresponds to an increase in the [S/(I + C)] ratio, indicating direct control of the monsoon over the clay mineral composition of sediments. By contrast, no link was found with glacial/interglacial cycles. In their work, Boulay *et al.* (2005) confirmed that the [S/(I + C)] ratio can be used as proxy to reconstruct variations in Southeast Asian monsoon intensity in the northern part of the SCS.

North Atlantic Ocean: deep oceanic currents and glacial/interglacial variability

Site description

The northern North Atlantic basins play a key role in the formation of the North Atlantic Deep Water (NADW; Fig. 7), an essential component of the global thermohaline circulation that controls interhemispheric heat exchanges (Broecker & Denton, 1989). The NADW results from a combination of three components: the Northeast Atlantic Deep Water (NEADW), the Denmark Strait Overflow Water (DSOW) and the Davis Strait Overflow (DSO; Dickson & Brown, 1994; Lucotte & Hillaire-Marcel, 1994). The NEADW and DSOW are driven in an anticlockwise gyre from the southern tip of Greenland to the outlet of the Labrador Sea by the Western Boundary Undercurrent (WBUC; McCartney, 1992). The NADW, produced offshore from Newfoundland, first flows southwards, then mixes with Circumpolar Deep Water in the Southern Hemisphere and returns back to northern latitudes through the Indian and Pacific oceans (Broecker, 1991). Numerous studies have shown variable intensity of the NADW over glacial and interglacial cycles (e.g. Ledbetter & Balsam, 1985; Boyle, 1995; Barker *et al.*, 2010), but also over shorter (millennial) timescales (e.g. Bond *et al.*, 2001; Oppo *et al.*, 2003).

In the deep North Atlantic basins, clay minerals are mainly detrital, derived from the weathering of adjacent continental masses (Biscaye, 1965; Piper & Slatt, 1977; Zimmermann, 1982). The clay mineral assemblages in surface sediments of northern North Atlantic basins display a clear spatial distribution (Fagel *et al.*, 1996). The greatest abundances of smectite were observed in the Iceland (>60%; Fig. 7) and Irminger (57%; Fig. 7) basins. In the Labrador Sea, illite and chlorite were the most common clay minerals on the Canadian margin (29–39% and 21–29% respectively). They were associated with up to 30% vermiculite at shallow depths (≤530 m) but only traces of vermiculite at greater depths (>2650 m). Smectite, which was absent in the shallowest sites of the Canadian margins, occurred at greater depths (>2650 m) along both Labrador Sea margins. The greatest smectite abundance was measured on the continental rise of both Labrador Sea margins, within a water depth of 2800–3400 m, a depth interval consistent with the axis of maximum velocity of the WBUC. As a supply from the adjacent Greenland and Canadian margins is improbable, the WBUC is most probably responsible for the transport of smectite-rich material from the eastern Iceland and Irminger basins and for their sedimentation in the Labrador Sea (Fagel *et al.*, 1996). This observation shows that clay minerals may be used as proxies for deep circulation. The clay mineral variability in Labrador Sea sediments was therefore used as a proxy for deep-water sediment transport over glacial/interglacial cycles (Fagel *et al.*, 1997b; Fagel & Hillaire-Marcel, 2006).

Materials and methods

Three cores drilled in the Labrador Sea were analysed. ODP Site 646 (58012.26'N, 48°22.15'W) was located off Greenland, on the upper flank of the Eirik Ridge sediment drift, below the axis of maximum velocity of the WBUC (Fig. 7; Fagel & Hillaire-Marcel, 2006). Two cores – 646A (water depth of 3462 m) and 646B (water depth of 3459 m) – were combined into a composite section using magnetic and lithostratigraphic correlations (Srivastava *et al.*, 1987). The upper 150 cm of sediments are only made of biogenic carbonates. At greater depth, the sediments are made of clayey and silty muds with a variable abundance of detrital carbonate-rich sandy layers, interpreted as turbiditic

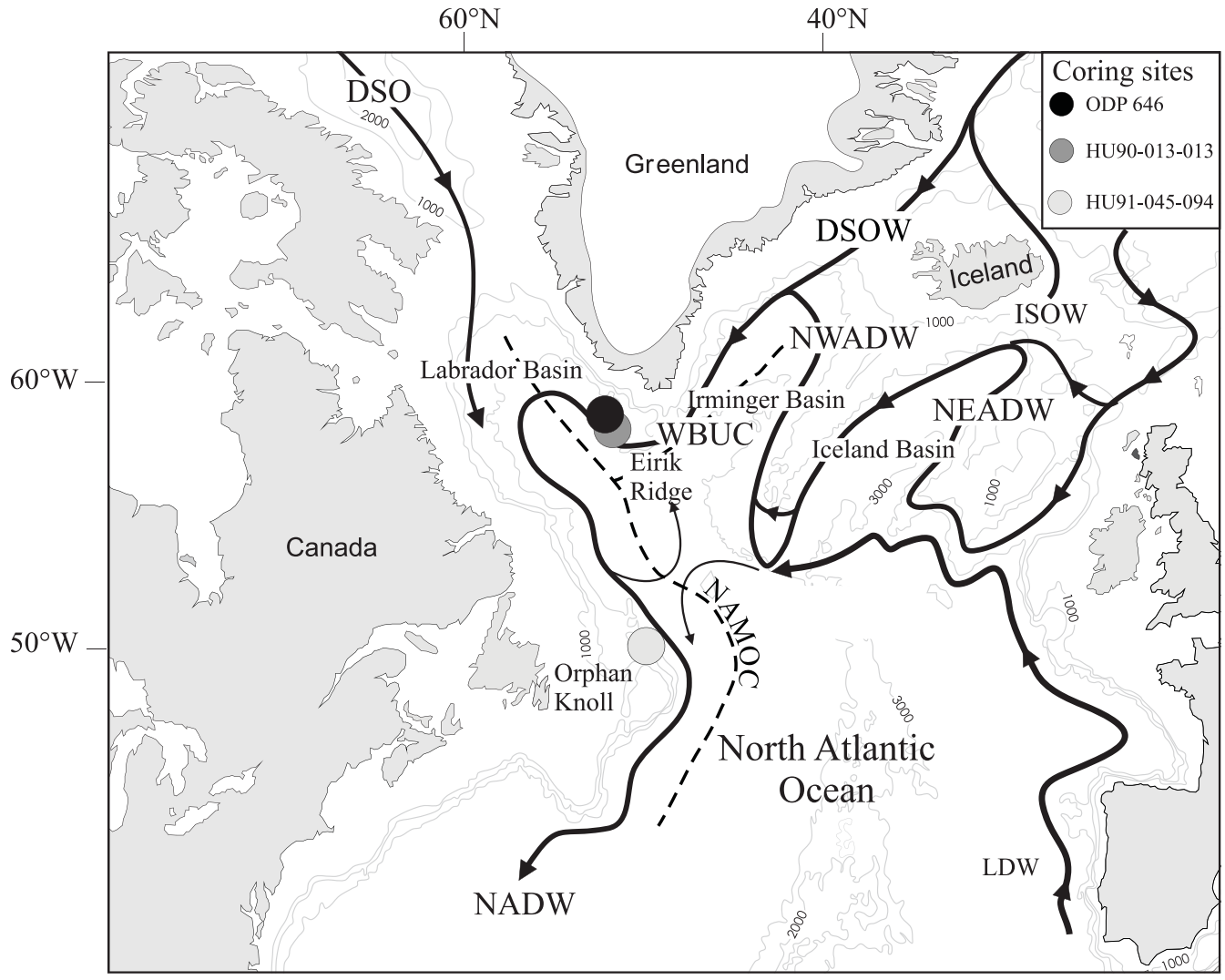

Figure 7. Locations of studied coring sites in the Labrador Sea. The deep circulation patterns in the northern North Atlantic basin are adapted from Dickson & Brown (1994) and Lucotte & Hillaire-Marcel (1994). The light grey lines indicate water depth. DSO = Davis Strait Overflow; DSOW = Denmark Strait Overflow Water; ISOW = Iceland Sea Overflow Water; NADW = North Atlantic Deep Water; NAMOC = North-West Atlantic Mid-Ocean Channel; NEADW = North-East Atlantic Deep Water; NWADW = North-West Atlantic Deep Water; WBUC = Western Boundary Undercurrent.

deposits. Oxygen isotope ratios measured from planktonic foraminifers were combined using biostratigraphy and magnetostratigraphy to define an age-depth model. The upper 32 m of core 646 were subsampled at 20 cm intervals (173 samples) for clay mineralogical analyses. This interval covered several glacial and interglacial periods, corresponding to the last 365 kyr (MISs 1–10). The sampling resolution was of 2500 years.

A second core (HU90-013-013; 58°12.59'N, 48°22.40'W) was collected on the south-west of Greenland Rise, north of the Eirik Ridge, at a water depth of 3380 m (Fig. 7). The site is bathed by DSOW overlain by NEADW (Lucotte & Hillaire-Marcel, 1994). The upper 530 cm of the core were composed of clayey silts and silty clays. Two sandy layers at 440–450 and 505–510 cm were interpreted as ice-rafted debris. Samples were retrieved between 240 and 530 cm, an interval covering the Last Glacial/Holocene transition (~8–26 kyr) according to the age model (Fagel *et al.*, 1997b). Sampling every centimetre provided a resolution between 10 and 160 years according to the sedimentation rate. The glacial interval (MIS2) was characterized by lower sedimentation rates (10 cm kyr^{-1}) than those of the Holocene interval (MIS1, > 30 cm kyr^{-1}; Hillaire-Marcel *et al.*, 1994).

A third core (HU91-045-094; 50°12.26'N, 45°41.14W) was retrieved from the southern Labrador Sea, in a deep channel on the Orphan Knoll at a water depth of 3448 m (Fig. 7). The bottom water mass is DSOW-like for core HU90-013-013. The 400 cm-long sediment core consisted of clays interlayered with abundant 10–40 cm-thick sandy layers. These layers displayed ice-rafted debris and a great detrital carbonate content, suggesting that ice surges on the Hudson Strait shelf (Andrews *et al.*, 1995) triggered turbidites to flow down the North Atlantic Mid-Ocean Channel corresponding to these sediment layers (see location in Fig. 7; Hillaire-Marcel *et al.*, 1994). Such events were interpreted as the final collapse of the Laurentide ice sheet (Andrews *et al.*, 1995). The core was subsampled at a lower resolution than core HU90-013-013 due to the presence of turbidite layers. A total of 68 samples were selected from 13 sediment intervals separating the turbidite layers.

For the three cores, the clay mineralogy was determined by XRD on the carbonate-free <2 µm fraction. Oriented mounts,

prepared according to the glass slide method (Moore & Reynolds, 1997), were analysed on a Siemens diffractometer with Co-*K*α radiation. Semi-quantitative estimation of clay minerals was derived from the peak areas of smectite (17 Å), illite (10 Å) and chlorite + kaolinite (7 Å) on the traces from the glycolated XRD mounts, determined by multiplying peak heights by widths at mid-height (Fagel *et al.*, 1997b). The peak heights of kaolinite at 3.57 Å and chlorite at 3.54 Å were measured to estimate their relative proportions (Biscaye, 1965). For the two cores located on the Greenland Rise (ODP646 and HU90-013-013), the clay mineral variation was expressed by the relative abundance of smectite and illite defined as their peak area ratio (S/I). In addition, the accumulation rates of smectite and illite (i.e. clay fluxes) were also evaluated by using Equation 1 (Fagel *et al.*, 1997b):

$$\text{Flux}_{\text{clay mineral (g/cm}^2\text{ kyr)}} = \delta \times \text{SAR} \times \%\text{clay mineral} \times \%\text{clay-sized fraction} \quad (1)$$

where δ is the mean clay mineral density (g cm^{-3}), SAR is the sediment accumulation rate (cm kyr^{-1}), % clay mineral is the abundance of the clay mineral in the fine <2 μm fraction determined by XRD and % clay-sized fraction is the proportion of the <2 μm fraction in the bulk sediment.

Results and interpretation

At ODP Site 646, the clay mineral assemblage comprises on average ~60% smectite, ~20% illite and similar proportions of chlorite and kaolinite (each ~10%; Fig. 7). According to the distribution of smectite in the surface sediments of the Iceland, Irminger and Labrador Sea basins, smectite was interpreted as being of distal origin, supplied by deep current from the eastern Irminger and Iceland basins, whereas illite and chlorite were proximal, delivered to the Labrador Sea from the erosion of the Greenland margin (Fagel *et al.*, 1996). Systematic changes were observed between glacial and interglacial intervals in core 646, where interglacials displayed greater abundance of smectite, except for the Holocene (40%), whereas glacial intervals showed a marked drop in smectite (≤40%) and a corresponding increase in illite and chlorite. Such variability indicated changes of mineral provenance over glacials/interglacials, with increased distal supplies of smectite by the deep WBUC from the smectite-rich Irminger and Iceland basins into the Labrador Sea (Fagel *et al.*, 1996). The relative clay mineral abundances were converted into clay fluxes (Fagel *et al.*, 1997b). The illite fluxes were systematically greater (×2) during glacial intervals than interglacial ones, recording greater contributions from the proximal Greenland margin. By contrast, the smectite fluxes remained stable over the last 365 kyr, indicating a constant supply by the deep currents from the more distal Irminger and Iceland basins. The surface sediments, however, displayed a marked increase in clay flux, which is probably due to the peculiar modern deep circulation conditions.

In core HU90-013-013 (Fig. 7), the smectite abundance averages 55% ± 10%, with a broad range of variation (20–75%). The illite abundance ranges between 10% and 45%, averaging 21% ± 6%. Smectite gradually increases over the Glacial/Holocene transition (14 kyr), whereas illite decreases. The S/I ratio increased by a factor of 4 between the Last Glacial Maximum (20 kyr) and the early Holocene, reaching a maximum at 9 kyr. The smectite flux increased by a factor of 7 above the Late Glacial/Holocene transition, reaching 28 g cm^{-2} kyr^{-1} in the uppermost studied sample (240 cm, early Holocene). By contrast, the range of variation for illite flux is narrow (2–9 g cm^{-2} kyr^{-1}). The observed increased supply of smectite at and above the Late Glacial/Holocene transition is consistent with increased distal smectite-rich sediment supplies from the eastern basins into the Labrador Sea. The maximum S/I ratio value at ~9 kyr probably reflects the rapid velocity of the WBUC.

At the outlet of the Labrador Sea, no modification of clay mineralogical composition occurred through depth/time in core HU91-045-014 (Fig. 7). Smectite ranged between 18% and 60% (average 38% ± 10%), with alternation occurring between smectite-rich and smectite-poor layers. The other clay minerals had a narrower range of variation (averages: illite 28% ± 5%, chlorite 19% ± 4%, kaolinite 15% ± 3%), with greater abundance than in core HU90-013-013 (Fagel *et al.*, 1997b). The smectite-rich layers had no carbonate sands, whereas the smectite-poor layers were carbonate-rich. Therefore, the generally lower abundance of smectite in core HU91-045-014 than in core HU90-013-13 is mainly due to dilution by detrital carbonate inputs originating from Hudson Bay (Andrews *et al.*, 1995). Therefore, in this case, low smectite abundance cannot be said to indicate a slower WBUC because the palaeocurrent information was erased by the carbonate deposits.

Clay variability in lacustrine sediments

Lake sediments (Table 2) represent valuable archives of past environmental changes on the continents, providing a continuous and sensitive record of changing conditions and processes occurring within lakes and in their surrounding catchments (Anselmetti *et al.*, 2006). Three types of minerals are present in lake sediments (Last, 2004). Detrital or allogenic minerals are brought into the lake *via* lake margin erosion, surface streams, landslides, slumping and/or aeolian dust. Endogenic minerals are formed in the water column by biologically induced or abiotic chemical precipitation. Authigenic minerals result from early diagenesis of sediment deposited at the lake bottom by chemical reactions in the interstitial waters of the sediments. In lakes, the geology of the watershed and the soil composition have greater influence on the detrital supplies than in marine environments (Boyle, 2004). Detrital minerals reflect the interaction between provenance, nature and intensity of weathering processes within the watersheds, tectonic settings and transport agents into the lake, and they are useful for tracking climate changes in the watersheds. The endogenic minerals probably indicate the chemical and limnological conditions of the water column at the time of mineral formation (Last, 2004). The interpretation of authigenic minerals, although more complex, may supply information on palaeoenvironmental conditions (Last, 2004). Moreover, water-level variations in lakes reflect the balance between precipitation and evaporation, recording climate changes (Last, 2004), especially in closed lakes (with inlets but without outlets). As for oceanic basins, an International Continental Scientific Drilling Program (ICDP) was launched in 1996, and, to date, ~60 drilling projects have been developed (Harms *et al.*, 2007).

Lake Baikal: glacial/interglacial variability and fluviatile supplies

Site description

The Baikal Drilling Program (BDP) was the first initiative, begun in 1993, of long coring in continental settings, and it was developed with the aim to provide a continental archive 'with the same scientific and chronostratigraphic integrity as marine

records' (Williams *et al.*, 2001). Located in south-central Siberia, Lake Baikal (Fig. 8) is the largest (636 km long × 79 km wide, 31.722 km^2) and deepest (1642 m) lake in the world. It is located in an active tectonic rift zone, unaffected by continental ice sheets and out of direct oceanic influence (Hutchinson *et al.*, 1992). Its thick sedimentary cover (up to 5000 m) records tectonic and climatic changes over the last 20–40 Myr (Williams *et al.*, 1997). Lake Baikal sediments constitute powerful archives of past climate over Plio-Pleistocene glacial/interglacial cycles for south-central Siberia over the past 5 Ma (Williams *et al.*, 1997; Grachev *et al.*, 1998; Kuzmin *et al.*, 2001). Coring sites in the southern (BDP-93; BDP-93 End-Members, 1995) and northern basins (BDP-96, BDP-98; Fig. 8; Grachev *et al.*, 1998; Karabanov *et al.*, 2000; Prokopenko *et al.*, 2002) showed that Lake Baikal sediments were sensitive to climate fluctuations because there was greater diatom abundance during interglacial intervals and lower diatom abundance during glacial intervals. Lake Baikal provided an interesting opportunity to test the use of clay minerals for palaeoclimatic interpretation in a continental environment (e.g. Yuretich *et al.*, 1999; Sakai *et al.*, 2005). At present, Lake Baikal is fed by 90% river supplies, 8% atmospheric supplies and 2% groundwater discharges (Lomonosov *et al.*, 1995). Lake Baikal is mainly supplied by three rivers: the Selenga River (2172 kT yr^{-1}) in the southern sector of the lake, the Barguzin River (178 kT yr^{-1}) on the eastern side of the lake and the Upper Angara River (430 kT yr^{-1}) in the northern sector of the lake (Fig. 8), supplying 94% of annual particulate input. The types of source rocks in the Lake Baikal watershed were characterized and quantified using spatial analyses of Geographic Information System datasets (Fagel *et al.*, 2007). Palaeozoic granitoids dominate the watershed of the Selenga River (56%) with Cenozoic volcanic rocks (16%), mainly basalts, Tertiary and Quaternary sedimentary rocks (11%) and metamorphic Precambrian schists (7%). Archaean and Proterozoic intrusive rocks dominate in the Barguzin (50%) and Upper Angara (40%) watersheds. In terms of mineralogy, illite is the predominant mineral, derived from the micas of Proterozoic and Archaean granites outcropping on the south-east margin of the lake (Galasy, 1993). Chlorite, the second detrital clay mineral in the catchment of Lake Baikal, is mainly sourced from the Proterozoic metamorphic belt (schists, quartzites) along the western flank of the lake, south of the Siberian platform. The composition of secondary minerals varies according to the rate of weathering, which is controlled by the composition of parental rocks, topography and climate (Chamley, 1989). Therefore, the lacustrine sediments are expected to present a variable mineralogy through time.

The long-term evolution of clay mineral assemblages over a few hundred thousand years was investigated at a few coring stations on Buguldeika Saddle (Melles *et al.*, 1995; Yuretich *et al.*, 1999) and Academician Ridge (Fagel *et al.*, 2003). Clay mineral data from BDP-93 cores from the Southern Central Basin (Yuretich *et al.*, 1999) showed that during the last 350 kyr there was a systematic increase of smectite in diatom-bearing sediments, indicating that a climate signature could be recorded in the clay-size fraction, which prompted further studies. Similarly to diatom productivity, the changes in smectite abundance were explained by temperature. Assuming all smectite is derived from soils, the observed trend by which smectite increased in warmer periods would reflect increased hydrolysis within the watershed during interglacials (Yuretich *et al.*, 1999). Subsequent studies are described here.

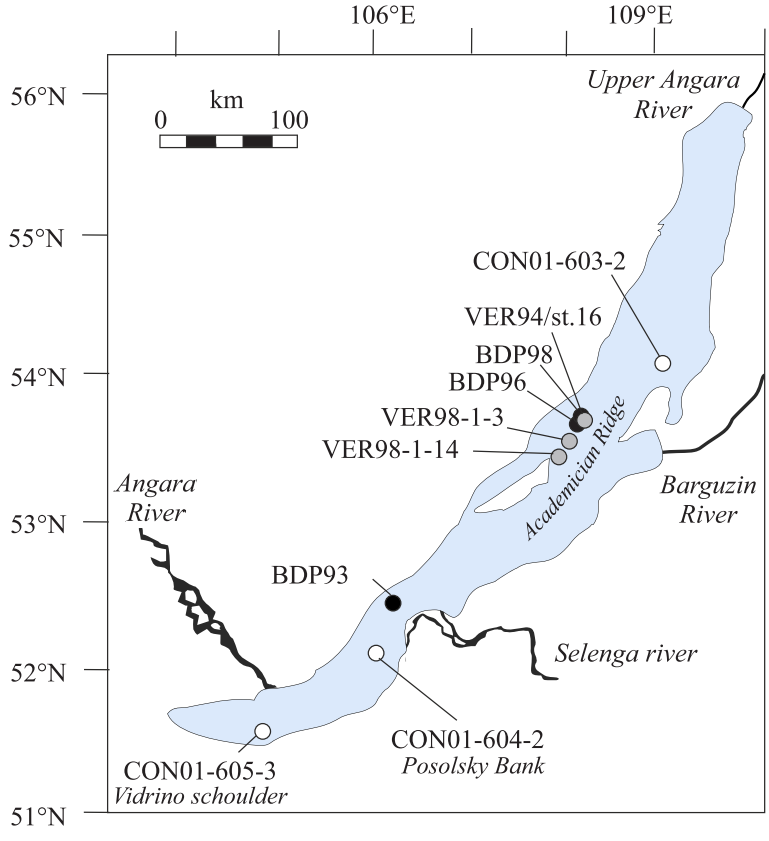

Figure 8. Coring locations in Lake Baikal from various drilling campaigns: BDP (black circles; Yuretich *et al.*, 1999; Williams *et al.*, 2001); VER (abbreviation derived from the name of the Russian vessel *RV Vereshagin*; grey circles; Horiuchi *et al.*, 2000; Fagel *et al.*, 2003); CON (Continent European proposal EVK2-CT-2000-00057; white circles; Fagel & Boës, 2008; Fagel & Mackay, 2008).

Materials and methods

Core VER98-1-3 was drilled on the northern part of Academician Ridge (53°44'56"N, 108°19'02"E) at a water depth of 373 m (Fig. 8). Academician Ridge is an intra-rift accommodation zone separating the central and north Baikal basins (Mats *et al.*, 2000). The total length of the core was 1092 cm, but its lower part (835–1092 cm) was disturbed during the coring and therefore not investigated further (Fagel *et al.*, 2003). The sediment was made of clayey silty layers interbedded with several decimetre-thick massive or faintly laminated diatom-rich layers. The diatom-rich intervals were attributed to warm (interglacial) intervals characterized by enhanced biological productivity. The clay-rich intervals that are either massive, coarsely to finely laminated or bioturbated (Fagel *et al.*, 2003) were associated with colder (glacial) intervals. In core VER98-1-3, the abundance of diatoms followed a pattern similar to the standard marine oxygen isotope curve (SPECMAP) that records glacial/interglacial fluctuations. In sediments from Lake Baikal, the correlation between the diatom content and SPECMAP, the latter calibrated with radiocarbon dates for the latest Quaternary and Holocene, was indeed used as a stratigraphic tool (Grachev *et al.*, 1998) to extrapolate further back in time (before 35 kyr). In this study, the age model was based on the correlation between the depths at which diatom assemblages VII–XV were found in reference sections from Academician Ridge (Likhoshway, 1998) and in core VER98-1-3. Assuming a constant sediment accumulation rate, the biostratigraphic correlation suggested that the last 54 kyr, corresponding to the uppermost 2.8 m of the sediments, are missing. The upper 8 m of core VER 98-1-3 probably recovered a time interval from 55 to 250 kyr, covering four interglacial/glacial intervals, labelled oxygen isotope stages (OISs) 4 to 8.

Core CON01-603-2a (53°96'N, 108°91'E, water depth of 386 m) was drilled in the northern basin of Lake Baikal on an extension of Academician Ridge called Continent Ridge (Fagel & Boës, 2007). The sediment from bottom to top was composed of silty clays with a few layers of diatoms (128–141 cm, unit 3), finely to coarsely laminated clayey silts to silty clays with abundant diatoms (9.5–128 cm, unit 2) and diffuse to finely laminated diatom-rich mud (0–9.5 cm, unit 1). The age model was derived from magnetic susceptibility and anhysteresis remanent magnetization measurements (Demory *et al.*, 2005) by correlation with the ODP 984 reference site (Noth Atlantic; Channell, 1999) using seven correlation points between 10.5 and 141.8 cm (Fagel & Boës, 2008). In core CON01-603-2a, the sedimentation rate averaged 10 cm kyr^{-1} in the middle unit (unit 2). The lowest sedimentation rates (~3.8 cm kyr^{-1}) were observed in unit 3 and at between 66 and 89 cm in unit 2. The entire core covered the last 22 kyr, with the Late Glacial/Holocene transition happening at 76 cm. The age of the surface sediments was estimated at 2.8 kyr BP by extrapolation of the youngest measured sedimentation rate.

Core CON01-604-2a (52.08°N, 105.86°E) was retrieved on Posolsky Bank (Fig. 8) in the vicinity of the Selenga River delta at a water depth of 133 m (Fagel & Boes, 2007). Posolsky Bank is a tilted fault block within the Selenga Delta Accommodation Zone (Hutchinson *et al.*, 1992). The sediments consisted of homogeneous silty clays at the bottom (105–110 cm, unit 3), coarsely to finely laminated silt (25–105 cm, unit 2) and homogeneous mud at the top unit (0–25 cm, unit 1). The palaeomagnetically derived age models for core CON01-604-2a (Demory *et al.*, 2005) were constrained by seven correlation points between 9 and 130 cm with the ODP984 reference site (Channell, 1999). In core CON01-604-2a, the sedimentation rates ranged between 6.5 and 9.2 cm kyr^{-1} in unit 2 and increased in both the upper and lower lithological units (11 cm kyr^{-1} in unit 1, 16 cm kyr^{-1} in unit 3). The entire core represented an interval ranging between 2.4 and 14 kyr, with the Late Glacial/Holocene transition occurring at 75–76 cm (Fagel & Boës, 2008).

The mineralogy of core VER98-1-3 was studied with XRD at low resolution (1 sample per 10 cm), whereas XRD analyses were performed at every centimetre in cores CON01-603-2a and CON01-604-2a, corresponding to an average temporal resolution of ~100 years. Qualitative and semi-quantitative estimations of clay mineral assemblages were based on XRD peak intensity measurements made on oriented, glycolated aggregates (Fagel *et al.*, 2003), and these analyses were also accompanied by those of air-dried and heated samples for comparison. XRD analysis was carried out on a Philips PW 1390 diffractometer using Cu-*K*α radiation. Smectite presence was indicated in two ways. First, illite–smectite was indicated by a shoulder of the low-angle side of a peak at 14 Å (Thorez, 1976). The abundance of this illite–smectite phase was estimated by the difference between the intensity of the 10 Å peak before and after heating (Boski *et al.*, 1998). Second, a peak was observed at ~17 Å on both the air-dried and glycolated samples. This behaviour is common in soils and was interpreted as being due to the presence of Al-hydroxides within the interlayers, called here Al-smectite (Thorez, 2000). The 10 Å peak indicated illite, while those at ~14 Å and ~7 Å indicated chlorite and kaolinite.

For clay mineral quantification, the intensity of the 10 Å peak was used as a reference and the peaks of the other minerals were divided by a weight factor (2.5 for 10–14 Å and chlorites, 1.4 for kaolinite, 5 for Al-smectite) and all identified clay species were normalized to 100%. These corrective factors were determined empirically at the University of Liège (J. Thorez, pers. comm. 2001). An S/I ratio was estimated on the glycolated diffractograms, reflected the abundance of illite–smectite and Al-smectite relative to illite. Assuming all smectites formed by transformation processes, the S/I ratio may be used as a proxy for hydrolysing conditions in the lake watershed (Fagel & Boës, 2008).

In addition, Li saturation was performed on samples from core VER98-1-3 to investigate the composition of smectite. The abundances of montmorillonite and beidellite were estimated by comparing the intensities of the 10 Å peak on the XRD runs of three Li-saturated samples (Thorez, 1998) as follows: montmorillonite = I(Li-300GL) – I(Li_N); beidellite = I(Li-300) – I(Li-300GL), where GL is glycerol solvation. The relative contribution of Al-smectite was based on the intensity of the 17 Å peak in the Li-300 trace, which was then reported on the glycolated trace (Fagel & Boës, 2007).

Results and interpretation

The mean clay mineral composition of core VER98-1-3 was 40% illite, 25% illite–smectite, ~3% Al-smectite, 16% kaolinite, 11% chlorite and 5% irregular mixed-layer illite–chlorite (Fagel *et al.*, 2003). The S/I ratio fluctuates by a factor of 4 throughout the core (Fig. 9a), with the highest values occurring during or near the termination of the diatom-rich intervals (reported as grey intervals in Fig. 9). The diatom-rich intervals, which indicated periods of greater productivity during warmer conditions (interglacial period), were usually characterized by greater abundance of beidellite (up to 14% in OIS 5e; Fig. 9c), with the warmer conditions favouring the transformation of mica/illite into beidellite (Fig. 9c). In most interglacial intervals, the greater

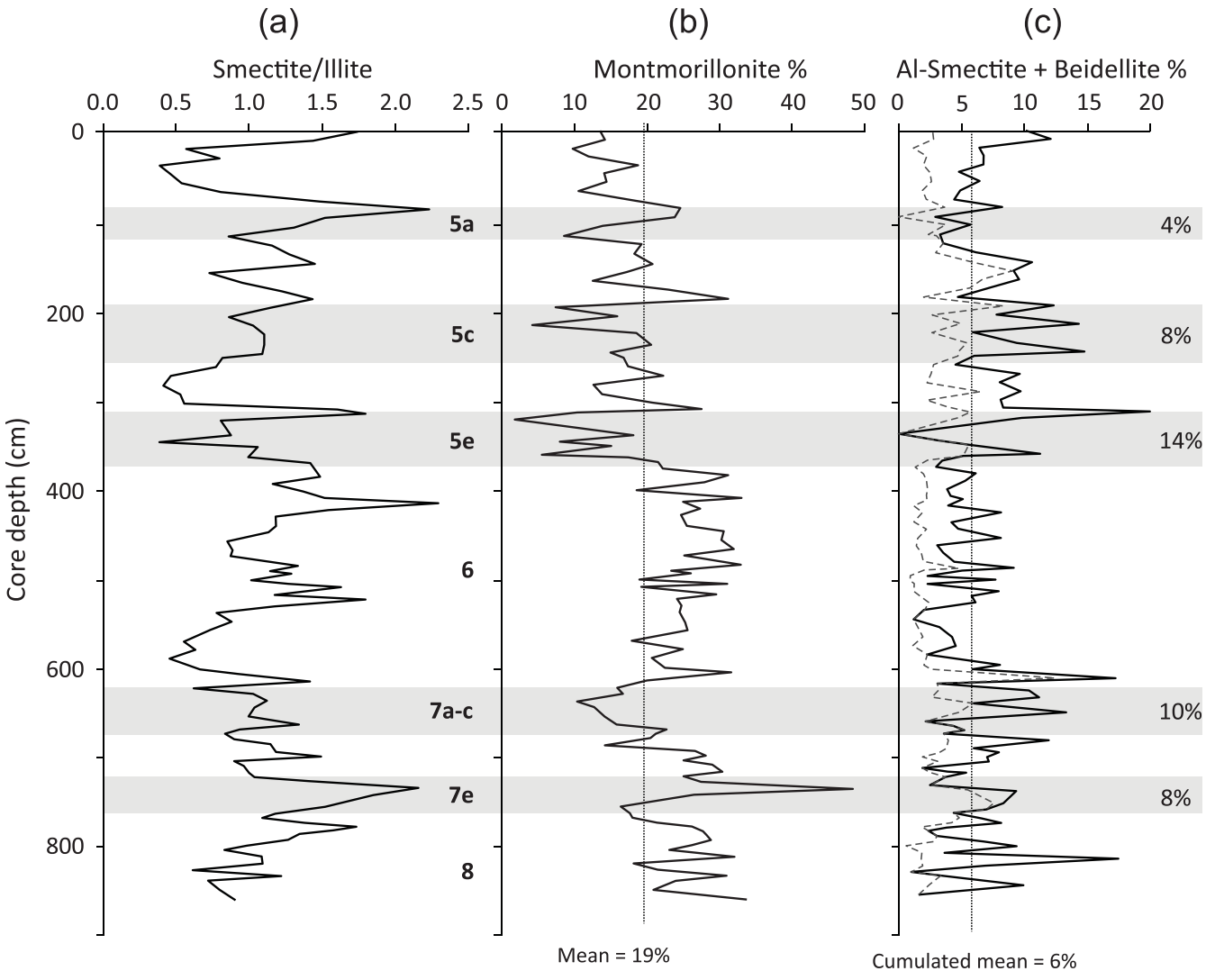

Figure 9. (a) Evolution of the smectite/illite ratio (17 $Å_{EG}$/10 $Å_{EG}$) with depth in core VER98-1-3. The grey bands indicate the interglacial intervals, and in white are the glacial periods, labelled according to the SPECMAP oxygen isotope stages. (b) Relative abundance of montmorillonite in the <2 μm size fraction. (c) Relative abundance of beidellite (continuous curve) and Al-smectite (dashed curve). The numbers in the right margin represent the cumulated contribution of beidellite and Al-smectite (in %) within the total clay fractions of interglacial intervals.

abundance of beidellite is associated with a slight increase in Al-smectite (Fig. 9c). Such hydroxy-interlayered minerals are common in soils with low levels of organic matter and that are stable in oxidizing and moderately acidic conditions (Rich, 1968; Meunier, 2007). By contrast, during glacial oxygen isotope stage 6, the relatively high S/I ratios record a greater contribution of montmorillonite (Fig. 9b). This could be explained by additional supplies of sedimentary smectites reworked by erosion from the watershed during glacial intervals. Those smectites were most probably derived from the erosion of Jurassic and/or Cretaceous sandstones and claystones outcropping in the Selenga River watershed (Fagel *et al.*, 2003). Therefore, only a part of the lacustrine clay assemblage appeared to record weathering conditions in the watershed. Generally, the climate significance of the proxy S/I ratio must be interpreted cautiously if reworked clay minerals are suspected.

The clay mineralogy in core CON01-604-2a (Fagel & Boes, 2007) consists of illite (mean 47% ± 6%), smectite (27% ± 6%), chlorite (14% ± 3%), kaolinite (8% ± 2%) and traces of illite–smectite (2% ± 1%). Its mean clay assemblage is close to the representative signature of Selenga River surface sediments, characterized by a 54% illite, 20% smectite, 13% chlorite, 7% kaolinite, 3% illite–smectite and 2% Al-smectite (Fagel *et al.*, 2007). Most of the clay mineralogy changes in core CON01-604-2a correspond to the opposing trends between smectite and illite (Fig. 10a). The S/I ratio ranges between 0.10 and 1.15, with a low mean value (0.4 ± 0.4) for the studied interval (Fig. 10b). After the Late Glacial/Holocene transition (~12.2 kyr), the S/I ratio curve has a minimum during the Boreal period (10.3–8.0 kyr) and then increases, reaching a maximum during the Subboreal period (5.7–2.6 kyr; Fig. 10b).

The clay record of core CON01-603-2a is composed of 37% ± 7% illite, 33% ± 8% smectite and 18% ± 5% chlorite (Fagel & Boes, 2007). There is no obvious change in the clay assemblage composition at the Late Glacial/Holocene transition (Fig. 10c). Moreover, the variation in smectite does not perfectly mirror that of illite (not shown), because chlorite in this core is a significant clay mineral, especially in the Holocene. The S/I ratio ranges between 0.1 and 2.7 (mean 0.8; Fig. 10c). The S/I ratio remains low (mean 0.6) in the Late Glacial period, except in a silty layer observed at

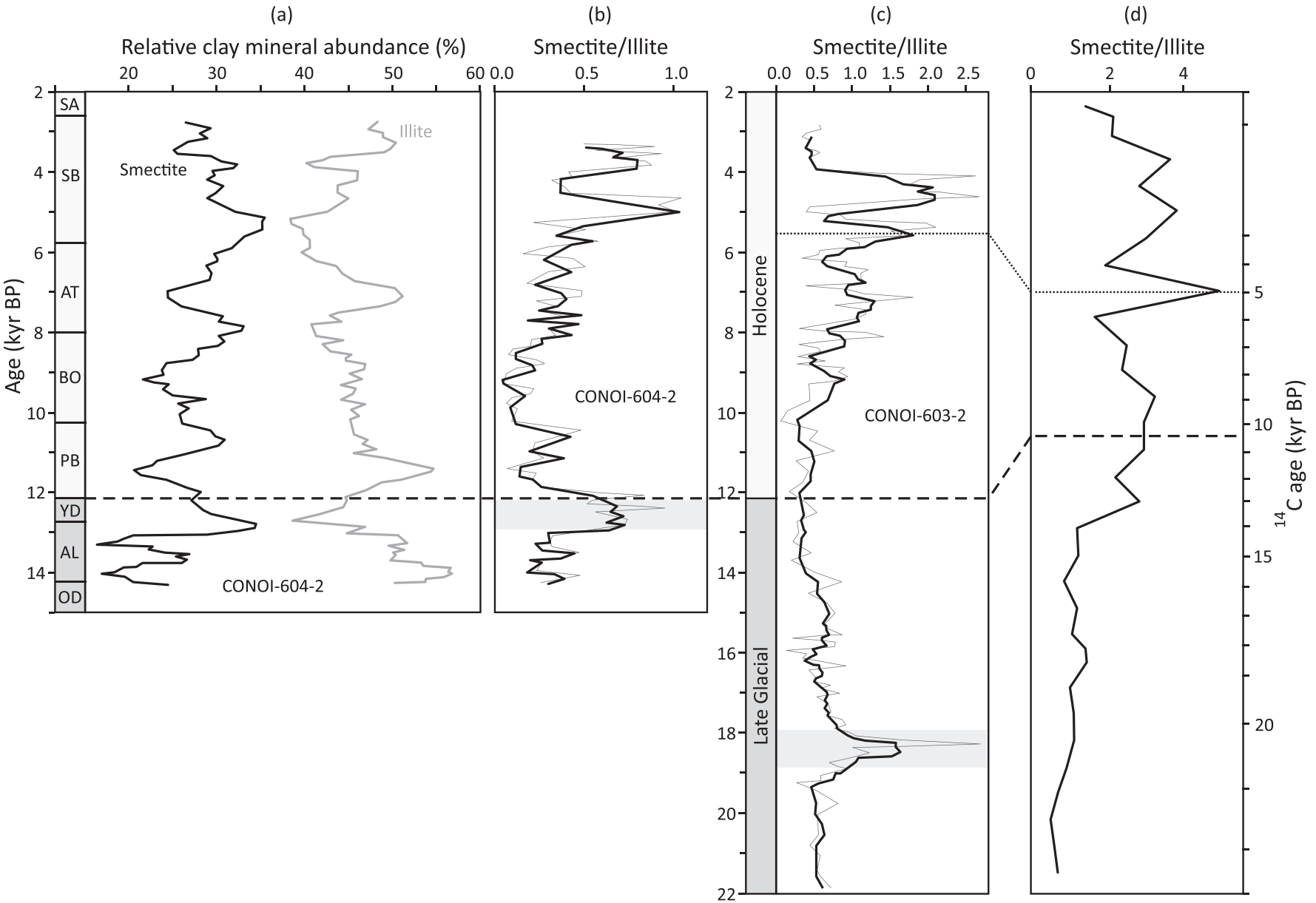

Figure 10. (a) Evolution of smectite and illite abundance in core CON01-604-2a. Each line represents a four-point running average of the sample data. (b) Evolution of the smectite/illite (S/I) ratio (17 $Å_{EG}$/10 $Å_{EG}$) in core CON01-604-2a. (c) Evolution of the S/I ratio in core CON01-603-2a. The bold line represents a four-point running average of the S/I value of the cores. The S/I increases (marked by a grey intervals) are not related to palaeoclimate but correspond to changes in the sediment lithology, most probably related to a change of source. The chronostratigraphy columns in (c) and (d) (Khotinsky, 1984) show the Late Glacial/Holocene transition, and in (a) and (b) they show the Younger Dryas/Preboreal transition (YD/PB; ~12.2 kyr BP; dashed line), the Preboreal/Boreal transition (PB/BO; ~10.3 kyr BP), the Boreal/Atlantic transition (BO/AT; ~8 kyr BP), the Atlantic/Subboreal transition (AT/SB; ~5.7 kyr BP) and the Subboreal/Subatlantic transition (SB/SA; ~2.6 kyr BP). (d) Evolution of the S/I ratio in core VER94/st.16 from the Academician Ridge (data from Horiuchi *et al.*, 2000).

18–19 kyr, where it reaches 1.8. After a minimum at the Preboreal/Boreal transition (10.3 kyr), the S/I ratio curve increases, although it is punctuated by several negative excursions. The maximum S/I ratio is reached during the Subboreal (~4.6 kyr) at 19 cm (Fig. 10c).

At both sites, S/I ratio values increase by a factor of 4 through the Holocene, reaching their maxima in the Subboreal (5.7–2.6 kyr). The S/I ratio followed a gradual but irregular increase throughout the Holocene. The slow warming over the Holocene period probably favoured the formation of smectite in Siberian soils. The highest S/I ratio values were also measured during the same Subboreal period in core VER94-16a recovered on Academician Ridge (Fig. 10d; Horiuchi *et al.*, 2000). Therefore, in the three cores (CON01-603-2, CON01-604-2 and VER94-16), the highest S/I ratios observed at ~5 kyr lag by ~2 kyr behind the optimal Siberian Atlantic climatic period (AT in Fig. 10a), which was identified in soils from the Lake Baikal area (Vorobyova, 1994) and in sedimentary palynological assemblages in Siberia (Schirrmeister *et al.*, 2002). This lag is probably due to the response time for soil re-equilibration.

To summarize, in Lake Baikal, the climate significance of clay assemblages at the scale of glacial/interglacial variability is mainly attested by a bimodal distribution between smectite (or illite–smectite) and illite caused by different clay sources and/or formation processes between cold glacial and warm interglacial periods. However, the variability at the millennial scale is less clear, possibly being affected by supplies of reworked sedimentary clays related to local tectonic events.

East African lakes: the palaeolake Chew Bahir – hydrological fluctuations related to arid and humid climate conditions

Site description

Since ~1970 CE, the East African Rift has been the subject of many palaeoanthropological and palaeoclimate studies searching for causal relationships between hominin evolution and climate changes (see Campisano *et al.*, 1997 for a review). Ethiopia in particular is characterized by an impressive accumulation of Pliocene fossil hominins (e.g. Johanson *et al.*, 1982) and late Pliocene flora and mammalian fauna (e.g. Bonnefille *et al.*, 2004; Reed, 2008).

Within this framework, an ICDP project (the Hominin Sites and Paleolakes Drilling Project; HSPDP) was launched to collect palaeoenvironmental data from lacustrine sediments close to key palaeoanthropological sites in Kenya and Ethiopia (Cohen *et al.*, 2009, 2016; Campisano *et al.*, 2017, Foerstner *et al.*, 2022). Among others, the Chew Bahir basin in south-west Ethiopia was analysed by Foerster *et al.* (2012) to reconstruct past environmental conditions and improve our understanding of the relationship between climate, environment and human dispersion in Africa. The Chew Bahir basin today is a dried-out saline mudflat laying in a transition zone between the Ethiopian Rift and the Omo-Turkana basin. This palaeolake was a closed basin (without any water outlet) receiving the totality of the weathering products from its catchment (Foertsner *et al.*, 2015). The western margin of the Chew Bahir basin is the Hammar range, which consists of Precambrian gneissic rocks. On the eastern margin, the Teltelee-Konso range contains Miocene basalts and trachytes. Oligocene basalts outcrop at the northern margin of the lake. The basin was infilled by ~5 km of sediments since the Miocene rifting. The fluviatile supplies are limited to the northern part of the basin, whereas the western and eastern margins are drained by rain. No sediments are supplied from the south lake margin. Sediment influx is seasonal, related to rainfall events during the wet season and to wind during the dry season, when it may become dominant.

Materials and methods

The core CB-01-2009 was recovered from the western margin of the Chew Bahir basin (04°50.6'N, 36°46.8'E) near an alluvial fan extending eastwards from the Hammar range (Foerster *et al.*, 2012). The sediment core covers the uppermost 18.86 m of the deposits, corresponding to ~45 kyr according to six radiocarbon age measurements (mean sedimentation rate 0.7 mm yr^{-1}). The lithology consists of silty clays intercalated with sandy layers and gravels. CB-01 records climate history spanning from 44 to 1.0 kyr, which includes the Last Glacial Maximum (18–23 kyr) and the African Humid Period (5–15 kyr) and ends at the onset of the Medieval Warm Period (700–1000 BP/950–1250 CE). The mineral content was determined by XRD analysis of bulk samples, using a Siemens D5000 diffractometer and the software *EVA* (Bruker) for qualitative phase identification. Elementary composition of the sediment core was determined by X-ray fluorescence with an Itrax core scanner (CS-XRF) equipped with a molybdenum tube. The core was scanned at 0.5 cm resolution with a voltage of 30 kV and a current intensity of 30 mA, with a scanning time per step of 20 s. The clay fraction was separated according to the protocol of Moore & Reynolds (1997) and analysed on an EMPYREAN PANalytical XRD device using Cu-*K*α radiation. Three diffractograms were measured on oriented mounts for each sample (air-dried, ethylene glycol-solvated and heated at 550°C for 2 h). The phase identification was performed using *HighScore Plus* version 4.0 software.

Results and interpretation

The bulk mineralogy of core CB-01 consists mainly of illite associated with K-feldspars (orthoclase and sanidine). A mineralogical study of the clay fraction was performed for the last 20 kyr recorded on core CB-01 (Fig. 11). Its clay mineralogy varied between illite-rich and smectite-rich intervals including mixed-layer illite–smectite (Fig. 11; Foerster *et al.*, 2018). The different mineral compositions were interpreted to correspond to dry or wet climate. Groups corresponding to each of these two climates were established by CS-XRF of the cores, corresponding to high and low K content, respectively (Foerstner *et al.*, 2012). High K content would mean arid, unfavourable living conditions for humans, whereas low K content would indicate more favourable, humid conditions (Foerster *et al.*, 2015). Such an interpretation is based on the transformation of smectite into authigenic illite during low lake levels. With more evaporation, the lake became more saline, favouring the formation of authigenic illite (Deocampo *et al.*, 2010) by smectite illitization. Such a process was confirmed by the migration of the 060 XRD reflection from 1.517 Å (dioctahedral Al-smectite) to 1.533 Å (trioctahedral Mg-illite) indicating higher water salinity, as well as the higher proportion of illite in the corresponding samples (Foerstner *et al.*, 2018). The mineralogical results for the Chew Bawir basin confirmed marked climatic phases, such as the African Humid Period (15–5 kyr; cf. samples CB01-7a-544 and CB01-7b-616 in Fig. 11; Foerster *et al.*, 2018).

East African lake: the palaeolake Lukeino in the Gregory Rift, Kenya – drainage intensity related to arid and humid conditions

Site description

The East African Rift valley is an active tectonic area with a particularly intense phase of rifting from the Cretaceous to the

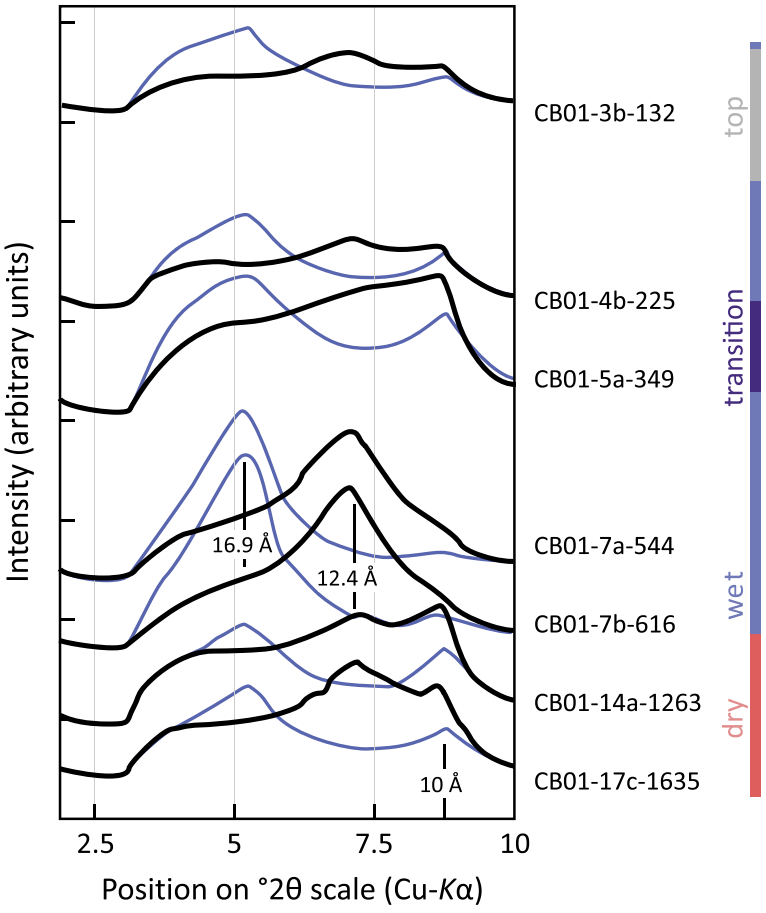

Figure 11. Comparison of XRD traces of air-dried (black curves) and ethylene glycol-solvated (blue curves) samples from oriented mounts of the fine fraction of CB-01 samples. The sample names are reported on the right. The last number in the labels corresponds to the core depth in centimetres. Three climate groups are assigned according to CS-XRF data: dry, wet and transition. The samples display a greater smectite proportion (best observed in the 16.9 Å peaks of ethylene glycol-solvated samples) in the wet climate phase. Modified from Foerstner *et al.* (2018).

Miocene, leading to the formation of numerous graben lakes (Tiercelin & Lezzar, 2002; Pickford *et al.*, 2009) filled with lacustrine and fluviatile sedimentary deposits and later with Middle Miocene to recent volcanic rocks. Fault reactivation in the Tugen Hill area was responsible for the formation of the Lukeino depression in which the palaeolake Lukeino developed (Pickford, 1974). The base of the formation is made by the Kabernet trachyte of 6.09 ± 0.14 Myr. The Lukeino Formation is sealed by the Kaparaina basalts (5.68 ± 0.18 Myr) that filled the depression and obliterated the palaeolake (Pickford, 1978; Sawada *et al.*, 2002).

The Lukeino Formation outcrops along the central part of the East African Rift, east of the Tugen Hills in Kenya, over an area 44 km wide × 13 km long (Bamford *et al.*, 2013). Sawada *et al.* (2002) proposed a simplified lithological column of the Lukeino Formation, divided into three members from bottom to top: (1) the Kapgoywa Member between the Kabernet trachyte and the Kapsomin basalt; (2) the Kapsomin Member; and (3) the Kapcheberek Member located between the Rormuch Sill and the Kaparaina basalt (Fig. 12). The Lukeino Formation was interpreted as a fluvio-lacustrine sedimentary sequence made by clayey and sandy clayey deposits intercalated by the Kapsomin basalts and the injection of the Rormuch Sill (Fig. 12; Pickford, 1975, 1978). This formation has yielded numerous floral, faunal and hominid remains (Bamford *et al.*, 2013) and it is known for revealing the oldest East African bipedal hominid, called *Orrorin tugenensis* (Senut *et al.*, 2001). This formation was investigated in detail to better constrain the environment in which the hominids lived (e.g. Pickford *et al.*, 2009; Bamford *et al.*, 2013).

Materials and methods

Sedimentary samples were collected in 2004, 2010 and 2011 within the framework of the 'Kenya Paleontological expedition' lead by B. Senut and M. Pickford from the National Natural History Museum of Paris in France. In total, 14 geological sections from six sites (Aragai, Cheboit, Kapgoywa, Kapsomin, Kapcheberek and Sunbarua) were investigated to cover the whole sequence of the Lukeino Formation (Dericquebourg, 2016). The sampling interval ranged between 0.1 and 1.0 m. The bulk mineralogy was studied on 480 horizons using a Bruker AXS D2-phaser equipped with Cu-*K*α radiation and a rapid LynxEye detector (ISTeP, Université Pierre et Marie Curie, Paris). The analyses were carried out between 2 and 75°2θ, with a step of 0.02°2θ and a counting time of 0.1 s per step, using a voltage of 30 kV and a current intensity of 10 mA. XRD traces were analysed using *MacDiff* software (Petschick, 1997). The semi-quantitative abundance of the minerals was derived from the measurement of peak surface, with an uncertainty of ±5% (Moore & Reynolds, 1997). Concerning the clay minerals, a kaolinite/smectite ratio was calculated from the surface ratios of the 001 peaks of kaolinite (7 Å) and smectite (15 Å) observed on the bulk XRD trace. This ratio was used to identify well-drained periods characterized by greater abundance of kaolinite over smectite (K/S > 1) and dry periods marked by the greater presence of smectite (K/S < 1), following a mineralogical study of Late Miocene fluvio-lacustrine deposits on the Ethiopian Plateau (Yemane *et al.*, 1987). In this study, the formation of both kaolinite and smectite was related to pedogenetic processes, as their distribution was not correlated with the presence

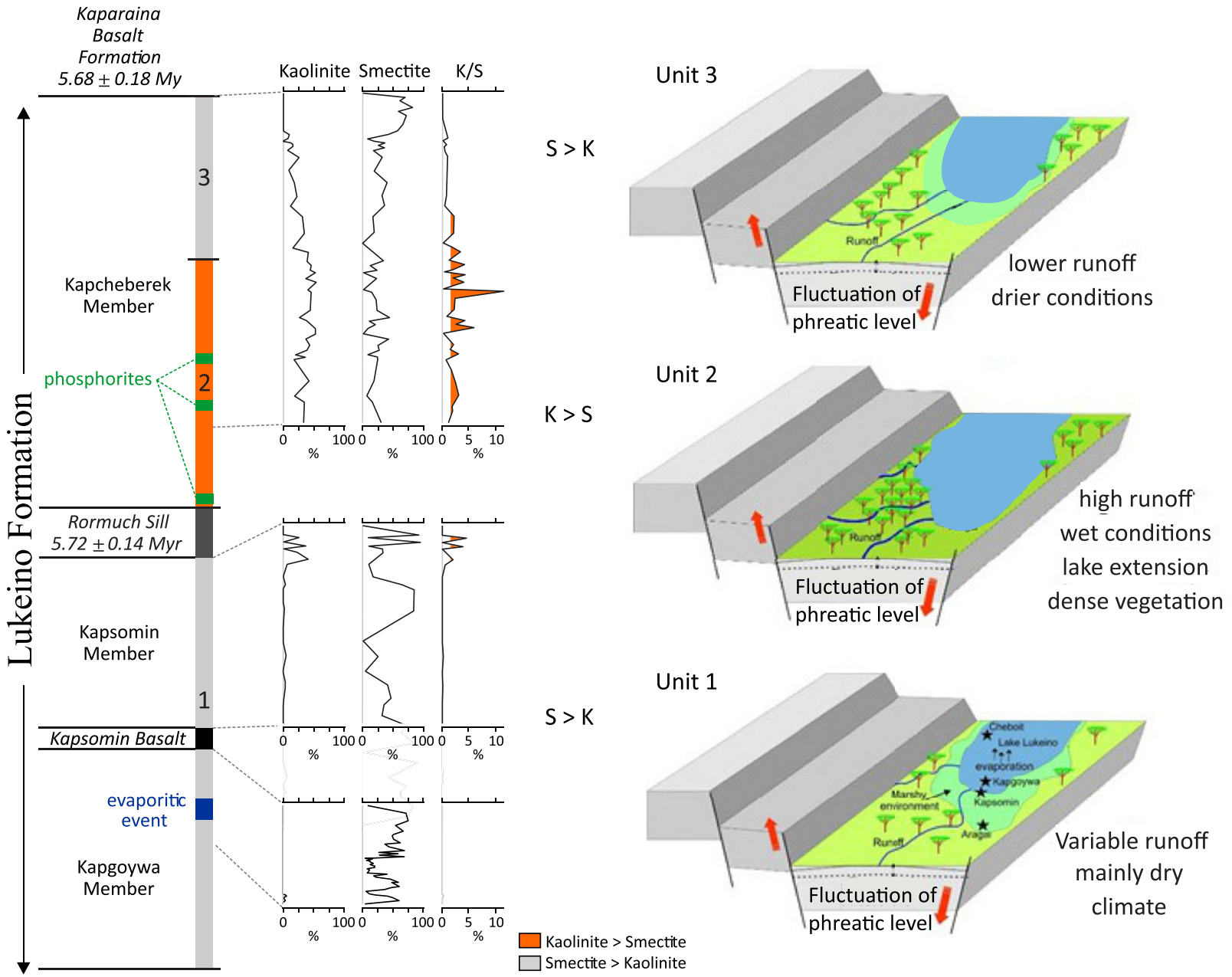

Figure 12. (Left) Evolution of the mineralogical assemblages of the Lukeino Formation derived from bulk XRD. The stratigraphic positions of the three Kapgoywa, Kapsomin and Kapcheberek members were based on lithological observation, magnetic susceptibility measurements and positions of the volcanic rocks. (Right) Palaeoenvironmental interpretation of the Lukeino sedimentary deposits derived from the peak area ratio between smectite and kaolinite (modified from Dericquebourg, 2016). The units correspond to sections 1, 2 and 3 on the left. K = kaolinite; S = smectite.

of volcanic materials. In soils, kaolinite is abundant in high-relief areas and/or in warm and humid environments formed under efficient drainage increasing the removal of cations and a portion of the dissolved silica (Millot, 1970; Chamley, 1989). Smectite is generally abundant in low-relief areas, where poor drainage prevents the removal of cations and silica. Its formation in soils is favoured by alternating wet and dry periods (Millot, 1970; Chamley, 1989). Therefore, for the Ethiopian sedimentary sequence, Yemane *et al.* (1987) emphasized that intense rainfall favoured the formation and the subsequent erosion of kaolinitic soils, whereas smectite-rich soils are instead developed during drier periods. The same interpretation was applied for the Lukeino Formation, as presented below.

Results and interpretation

The evolution of the mineralogical assemblages of the Lukeino Formation and, in particular, the evolution of the K/S ratios indicated several changes in the palaeoenvironmental conditions of the catchment of the palaeolake Lukeino (Fig. 12; modified from Dericquebourg, 2016). Three periods were identified:

(1) The first period (unit 1 in Fig. 12), was characterized by the absence or very low abundance of kaolinite (5%). Kaolinite was only present (up to 40%) as a major phase at the top of the Kapsomin Member (Fig. 12). Smectite was abundant (up to 60%) in the clay and silty clay layers across the sequence, with an average abundance of 45%. The K/S ratio was close to 0 in the greatest part of the sequence, except in the upper part, where the proportion of kaolinite is greater than smectite in several horizons ($1.9 < K/S < 4.4$). The low K/S ratio in unit 1 suggested a generally dry environment, with one peculiar stratigraphic interval characterized by intense evaporation (i.e. evaporitic layer in unit 1 in Fig. 12).
(2) The second period (unit 2 in Fig. 12) contained a high proportion of smectite (mean 60%) in the clay to silty clay layers. The kaolinite varied in the opposite way to smectite, with more kaolinite (30%) in the coarsest layers and less kaolinite (5%) in the finest layers. The K/S ratio displayed higher values than in unit 1, with a mean of 3.0 and a maximum of 11.5. The high proportion of kaolinite, associated with a greater content of quartz, suggested intense runoff with significant detrital supplies. This second interval coincided most probably with a well-drained phase. Moreover, the occurrence of phosphorite layers (Fig. 12), which were only observed in this period, emphasized the presence of dense vegetation in the watershed of the palaeolake (Dericquebourg *et al.*, 2015).
(3) The K/S ratio progressively decreased in unit 3 (Fig 12), ranging between 0.9 and 0 (mean 0.3). The decrease in kaolinite was interpreted as a return to drier conditions, leading to a drop in the lake level. Among the other non-clay minerals, this unit was marked by an increase in sanidine, a K-feldspar of volcanic origin. Its occurrence must be related to the pyroclastic deposits. The bulk mineralogy was also characterized by a lower abundance of quartz than in the other units, suggesting limited runoff during unit 2. Finally, the drier conditions (indicated by the low K/S ratio and low quartz abundance) and the volcanic activity (indicated by the presence of sanidine), related to the eruption of lavas of the Kaparaina basalts, were responsible for the sealing of the palaeolake Lukeino (Dericquebourg *et al.*, 2015; Dericquebourg, 2016).

The clay mineralogical study in palaeolake Lukeino provides complementary information regarding the Miocene palaeoenvironments where hominids lived. Dericquebourg (2016) showed that the lower part of the Lukeino Formation, encompassing the Kapgoywa and the Kapsomin members, was characterized by rather dry conditions, in agreement with the interpretations of the carbon and oxygen isotopic compositions of the teeth of herbivores contemporary with *Orrorin tugenesis* (Roche *et al.*, 2013). However, divergent conclusions were proposed for the Kapcheberek Member: more humid according to Roche *et al.* (2013), but drier according to Dericquebourg (2016).

Synthesis

Here are reported some points to consider in clay mineral analysis:

- The use of clay minerals as a climate proxy is mainly valid for Cenozoic sediments for two main reasons: (1) Cenozoic sedimentation is less affected by burial diagenesis; and (2) the Cenozoic active tectonic and cold climate conditions favoured physical erosion, supplying greater detrital fluxes.
- Climate information may be derived either from clay mineral abundance in bulk or <2 μm fractions, the height or surface peak ratio between two clay minerals or the abundance ratio between two or three clay minerals. Among those approaches, the measurement on XRD traces of peak height or surface ratio between two minerals is the most objective, as it is not influenced by the method of quantification of the clay minerals. It is therefore difficult to compare the clay mineralogical results from different studies. The relative abundance of clay minerals is more robust than absolute values for comparison.
- The abundance of clay minerals is dependent on the analysed grain size. In most studies, the clay mineral assemblage is identified on the fine <2 μm fraction that usually concentrates the clay minerals. However, some clay minerals may belong to the fine silt fraction. The XRD analysis of the bulk sediment is an alternative approach that would account for all clay minerals, whatever their particle size. Mineralogical quantitative XRD bulk powder methods have been significantly improved over the last decade.
- Clay assemblages may contain clay minerals reworked from sedimentary outcrops rather than being formed during the studied periods. These clays must be identified, as they may provide misleading information regarding the climate. However, as clay minerals may be transformed under new climate and basin conditions, they may still prove of value.
- Climate control of clay mineral sedimentation has been demonstrated through the detection of changes in clay composition over periods in the range of the Earth's orbital parameters (eccentricity, obliquity and precession). However, linking clay sediments to orbital parameters requires accurate knowledge of their deposition ages. Moreover, the duration of the studied interval must be at least five times longer than the supposed time cycles to enable their robust interpretation.
- The interpretation of sedimentary clay minerals is made easier if the source areas and transport agents are known. Clay minerals are significantly controlled by the watershed conditions in proximal deposition environments, such as deltas. These controls are easiest to decipher in sediment basins where two source areas are characterized by two distinct clay mineralogies and different transport agents operate from each source. When

several sources are involved, the use of isotopic tracers usually allows us to identify their potential sources.
- The numerous marine and lacustrine drilling projects conducted worldwide represent an impressive and interesting database from which to conduct further clay mineralogical studies on Cenozoic sediments.

Dedication. This manuscript is dedicated to the professors and researchers who initiated me into the world of clay minerals. In particular, I would like to thank professors Hervé Chamley and Pierre Debrabant from the University of Lille 1 (France), as well as Luc André, professor at the Université Libre of Brussels and researcher at the Royal Museum for Central Africa (Belgium). I completed my complementary master's degree (DEA) under the supervision of H. Chamley (1989–1990), then I joined his research team to perform my PhD thesis with P. Debrabant as promotor (1990–1993). L. André, who was already associated with my master's thesis at Université Libre of Brussels (1988–1989), was always present to give me advice on difficult career choices.

Acknowledgements. I thank all of the collaborators – professors, scientists, technicians and students – who have helped me over the years to deepen my understanding of the clay toolbox and its applications. This research was supported by both national (e.g. University of Liege, FNRS, WBI, BELSPO) and international (e.g. MRT France, CRSNG Canada, EU) funding agencies. Marttiina Rantala and Valentine Piroton are warmly thanked for their significant support in the preparation of the figures. I also acknowledge the two anonymous reviewers, the associate editor, Javier Cuadros, and the principal editor of *Clay Minerals*, George Christidis, for their positive comments and suggestions that allowed me to improve the text.

Conflicts of interest. The author declares none.

References

Adkins J.F., Boyle E.A. & Keigwin L.D. (1995) Sediment flux variations over the past 30 000 years at the Bermuda Rise. *Eos Transactions*, **76**, F282.

Alt J.C. & Jiang WT (1991) Hydrothermally precipitated mixed-layer illite–smectite in recent massive sulfide deposits from the sea floor. *Geology*, **19**, 570–573.

Andrews J.T., MacLean B., Kerwin M., Manley W., Jennings A.E. & Hall F. (1995) Final stages in the collapse of the Laurentide icesheet, Hudson Strait, Canada, NWT: ^{14}C AMS dates, seismic stratigraphy, and magnetic susceptibility logs. *Quaternary Research*, **14**, 983–1004.

Anselmetti F.S., Ariztegui D., Hodell D.A., Hillesheim M.B., Brenner M., Gilli A. *et al.* (2006) Late Quaternary climate-induced lake level variations in Lake Peten Itza, Guatemala, inferred from seismic stratigraphic analysis. *Palaeogeography, Palaeoclimatology, Palaeoecology*, **230**, 52–69.

Aoki S., Kohyama N. & lshizuka T. (1991) Sedimentary history and chemical characteristics of clay minerals in cores from the distal part of the Bengal Fan (ODP 116). *Marine Geology*, **99**, 175–185.

Bamford M.K., Brigitte Senut B. & Pickford M. (2013) Fossil leaves from Lukeino, a 6-million-year old formation in the Baringo Basin, Kenya. *Geobios*, **46**, 253–272.

Barker S., Knorr G., Vautravers M., Diz P. & Skinner L.C. (2010) Extreme deepening of the Atlantic overturning circulation during deglaciation. *Nature Geosciences*, **3**, 567–571.

BDP-93 End-Members (1995) Results of the first drilled borehole at Lake Baikal near the Buguldeika Isthmus. *Russian Geology and Geophysics*, **36**, 3–32 [in Russian].

Beaufort L. (1996) Dynamics of the monsoon in the equatorial Indian Ocean over the last 260,000 years. *Quaternary International*, **31**, 13–18.

Berger A. (1977). Support of the astronomical theory of climate change. *Nature*, **269**, 44–45.

Berger A. (2012) A brief history of the astronomical theories of paleoclimates. Pp. 107–129 in: *Climate Change: Inferences From Paleoclimate and Regional Aspects* (A. Berger, F. Mesinger & D. Sijacki, editors). Springer, Vienna, Austria.

Bergmann J., Friedel P. & Kleeberg R. (1998) *BGMN* – a new fundamental parameter-based Rietveld program for laboratory X-ray sources, its use in quantitative analysis and structure investigations. *CPD Newsletter*, **20**, 5–8.

Biscaye P.E. (1965) Mineralogy and sedimentation of recent deep-sea clay in the Atlantic Ocean and adjacent seas and oceans. *GSA Bulletin*, **76**, 803–832.

Bish D.L. & Chipera S.J. (1988) Problems and solutions in quantitative analysis of complex mixtures by X-ray powder diffraction. *Advances in X-Ray Analysis*, **31**, 295–308.

Blackman R.B. & Tuckey G.W. (1958) *The Measurement of Power Spectra*. Dover Publications, Inc., New York, NY, USA, 190 pp.

Bond G., Kromer B., Beer J., Muscheler R., Evans M.N., Showers W. *et al.* (2001) Persistent solar influence on North Atlantic climate during the Holocene. *Science*, **294**, 2130–2136.

Bonnefille R., Potts R., Chalie F., Jolly D. & Peyron O. (2004) High-resolution vegetation and climate change associated with Pliocene *Australopithecus afarensis*. *Proceedings of the National Academy of Sciences of the United States of America*, **101**, 12125–12129.

Boski T., Pessoa J., Pedro P., Thorez J., Dias J.M.A. & Hall I.R. (1998) Factors governing abundance of hydrolyzable amino acids in the sediments from the N.W. European Continental Margin (47–50°N). *Progress in Oceanography*, **42**, 145–164.

Boulay S., Colin C., Trentesaux A., Frank N. & Liu Z. (2005) Sediment sources and East Asian monsoon intensity over the last 450 ky. Mineralogical and geochemical investigations on South China Sea sediments. *Palaeogeography, Palaeoclimatology, Palaeoecology*, **228**, 260–277.

Boulay S., Colin C., Trentesaux A., Pluquet F., Bertaux J., Blamart D. *et al.* (2003) Mineralogy and sedimentology of Pleistocene sediment in the South China Sea (ODP Site 1144). Pp. 1–21 in: *Proceedings of the Ocean Drilling Program, Scientific Results* (W.L. Prell, P. Wang, P. Blum, D.K. Rea & S.C. Clemens, editors), **184**, 1–21. [Online]. Retrieved from: http://www-odp.tamu.edu/publications/184_SR/VOLUME/CHAPTERS/211.PDF

Bouquillon A., Chamley H. & Frohlich F. (1989) Sédimentation argileuse au Cénozoïque supérieur dans l'Océan Indien nord-oriental. *Oceanologica Acta*, **12**, 133–147.

Bouquillon A., France-Lanord C., Michard A. & Tiercelin J.-J. (1990) Sedimentology and isotopic chemistry of the Bengal Fan sediments: the denudation of the Himalaya. Pp. 43–58 in: *Proceedings of the Ocean Drilling Program, Scientific Results* (J.R. Cochran, D.A.V. Stow, C. Auroux, K. Amano, P.S. Balson & J.J. Boulègue *et al.*, editors), **116**. Ocean Drilling Program, College Station, TX, USA.

Bout-Roumazeilles V. (1995) *Relations entre les variabilités minéralogiques et climatiques enregistrées dans les sédiments de l'Atlantique nord pendant les huit derniers stades glaciaires-interglaciaires*. PhD thesis, Université de Lille I, Lille, France, 280 pp.

Bout-Roumazeilles V., Combourieu Nebout N., Peyron O., Cortijo E., Landais A. & Masson-Delmotte V. (2007) Connection between South Mediterranean climate and North African atmospheric circulation during the last 50,000 yr BP North Atlantic cold events. *Quaternary Science Reviews*, **26**, 3197–3215.

Boyle E.A. (1995) Last Glacial Maximum North Atlantic Deep Water: on, off or somewhere in between? *Philosophical Transactions of the Royal Society of London, Series A*, **348**, 243–253.

Boyle J.F. (2004) Inorganic geochemical methods in paleolimnology. Pp. 83–141 in: *Tracking Environmental Change Using Lake Sediments. Physical and Geochemical Methods*, vol. 2 (W.M. Last & J.P. Smol, editors). Kluwer Academic Publ., Dordrecht, The Netherlands.

Brass G.W. & Raman C.V. (1990) Clay mineralogy of sediments from the Bengal Fan. Pp. 35–41 in: *Proceedings of the Ocean Drilling Program, Scientific Results* (J.R. Cochran, D.A.V. Stow, C. Auroux, K. Amano, P.S. Balson & J.J. Boulègue *et al.*, editors), **116**. Ocean Drilling Program, College Station, TX, USA.

Broecker W. (1991) The great ocean conveyor belt. *Oceanography*, **4**, 79–89.

Broecker W.S. & Denton G.H. (1989). The role of ocean–atmosphere reorganisation in glacial cycle. *Geochimica Cosmochimica Acta*, **53**, 63–89.

Brown G. & Brindley G.W. (1980) X-ray diffraction procedures for clay mineral identification. Pp. 305–359 in: *Crystal Structures of Clay Minerals and Their X-Ray Identification* (G.W. Brindley & G. Brown, editors). Mineralogical Society, London, UK.

Butler B. & Hillier S. (2020) *powdR*: full pattern summation of X-Ray powder diffraction data. *R* package version 1.2.4. Retrieved from: https://CRAN.R-project.org/package=powdR

Butler B.M. & Hillier S. (2021) Automated full pattern summation of X-ray powder diffraction data for high-throughput quantification of clay-bearing mixtures. *Clays and Clay Minerals*, **69**, 38–51.

Cagatay M.N., Keigwin L.D., Okay N., Sari E. & Algan O. (2002) Variability of clay-mineral composition on Carolina Slope (NW Atlantic) during marine isotope stages 1–3 and its paleoceanographic significance. *Marine Geology*, **189**, 163–174.

Campisano C., Cohen A.S., Arrowsmith J.R. & Asrat A. (1997) The Hominin Sites and Paleolakes Drilling Project: high-resolution paleoclimate records from the East African Rift System and their implications for understanding the environmental context of hominin evolution. *PaleoAnthropology*, 1–43.

Campisano C., Cohen A.S., Arrowsmith J.R., Asrat A., Behrensmeyer A.K., Brown E.T. *et al.* (2017) The hominin sites and Paleolakes Drilling Project: high-resolution paleoclimate records from the East African Rift System and their implications for understanding the environmental context of hominin evolution. *Paleoanthropology*, **2017**, 1–43.

Casetou-Gustafson S., Hillier S., Akselssond C., Simonsson M., Stendahl J. & Olsson B.A. (2018) Comparison of measured (XRPD) and modeled (A2M) soil mineralogies: a study of some Swedish forest soils in the context of weathering rate predictions. *Geoderma*, **310**, 77–88.

Chamley H. (1989) *Clay Sedimentology*. Springer-Verlag, Berlin, Germany, 623 pp.

Chandler M.A., Rind D. & Ruedy R. (1992) Pangaean climate during the Early Jurassic: GCM simulations and the sedimentary record of paleoclimate. *GSA Bulletin*, **104**, 543–559.

Channell J.E.T. (1999) Geomagnetic intensity and directional secular variation at Ocean Drilling Program (ODP) site 984 (Bjorn Drift) since 500 ka: comparison with ODP983 (Gardar Drift). *Journal of Geophysical Research*, B104, 22937–22951.

Chen P.Y. (1978) Minerals in bottom sediments of the South China Sea. *GSA Bulletin*, **89**, 211–222.

Chipera S.J. & Bish D.L. (2002) *FULLPAT*: a full-pattern quantitative analysis program for X-ray powder diffraction using measured and calculated patterns. *Journal of Applied Crystallography*, **35**, 744749.

Clemens S.C. & Prell W.L. (1991) One million year record of summer monsoon winds and continental aridity from the Owen Ridge (Site 722), northwest Arabian Sea. Pp. 365–388 in: *Proceedings of the Ocean Drilling Program. Scientific Results* (W.L. Prell, N. Niitsuma, K.-C. Emeis, Z.K. Al-Sulaiman, A.N.K. Al-Tobbah, D.M. Anderson *et al.*, editors), **117**. Ocean Drilling Program, College Station, TX, USA.

Clemens S.C., Prell W.L., Murray D., Shimmield G. & Weedon G. (1991) Forcing mechanisms of the Indian Ocean monsoon. *Nature*, **353**, 720–725.

Cohen A., Arrowsmith R., Behrensmeyer A.K., Campisano C., Feibel C., Fisseha S., *et al.* (2009) Understanding paleoclimate and human evolution through the Hominin Sites and Paleolakes Drilling Project. *Scientific Drilling*, **8**, 60–65.

Cohen A., Campisano C., Arrowsmith R. & Asrat A. (2016) The Hominin Sites and Paleolakes Drilling Project: inferring the environmental context of human evolution from Eastern African Rift lake deposits. *Scientific Drilling*, **21**, 1–16.

Colin C., Turpin L., Bertaux J., Desprairies A. & Kissel C. (1999) Erosional history of the Himalayan and Burman ranges during the last two glacial–interglacial cycles. *Earth Planetary Sciences Letters*, **171**, 647–660.

Curray J.R., Emmel F.J. & Moore D.G. (2003) The Bengal Fan: morphology, geometry, stratigraphy, history and processes. *Marine Petroleum Geology*, **19**, 1191–1223.

Darby D.A. (1975) Kaolinite and other clay minerals in Arctic Ocean sediments. *Journal of Sedimentary Research*, **45**, 272–279.

De Menocal P., Bloemendal J. & King J. (1991) A rock-magnetic record of monsoonal dust deposition to the Arabian Sea: evidence for a shift in the mode of deposition at 2.4 Ma. Pp. 389–407 in: *Proceedings of the Ocean Drilling Program. Scientific Results* (W.L. Prell, N. Niitsuma, K.-C. Emeis, Z.K. Al-Sulaiman, A.N.K. Al-Tobbah, D.M. Anderson *et al.*, editors), **117**. Ocean Drilling Program, College Station, TX, USA.

Debrabant P., Fagel N., Chamley H., Bout V. & Coulet J.P. (1993) Neogene to Quaternary clay mineral fluxes in the Central Indian basin. *Palaeogeography, Palaeoclimatology, Palaeoecology*, **103**, 117–131.

Debrabant P., Krissek L., Bouquillon A. & Chamley H. (1991) Clay mineralogy of Neogene sediments of the western Arabian Sea: mineral abundances and paleoenvironmental implications. Pp. 183–196 in: *Proceedings of the Ocean Drilling Program. Scientific Results* (W.L. Prell, N. Niitsuma, K.-C. Emeis, Z.K. Al-Sulaiman, A.N.K. Al-Tobbah, D.M. Anderson *et al.*, editors), **117**. Ocean Drilling Program, College Station, TX, USA.

Deconinck J.F. & Vanderaveroet P. (1996) Eocene to Pleistocene clay mineral sedimentation off New Jersey, western North Atlantic (ODP Leg 150, Sites 903 and 905). Pp. 147–170 in: *Proceedings of the Ocean Drilling Program. Scientific Results* (G.S. Mountain, K.G. Miller, P. Blum, C.W. Poag & D.C. Twichell, editors), **150**. Ocean Drilling Program, College Station, TX, USA.

Demory F., Nowaczyk N.R., Witt A. & Oberhänsli H. (2005) High-resolution magnetostratigraphy of late Quaternary sediments from Lake Baikal, Siberia: timing of intracontinental paleoclimatic responses. *Global and Planetary Change*, **46**, 145–166.

Deocampo D.M., Behrensmeyer A.K. & Potts R. (2010) Ultrafine clay minerals of the Pleistocene Olorgesailie Formation, southern Kenya Rift: diagenesis and paleoenvironments of early hominins. *Clays and Clay Minerals*, **58**, 294–310.

Dera G., Pellenard P., Neige P., Deconinck J.F., Pucéat E. & Dommergues J.L. (2009) Distribution of clay minerals in Early Jurassic Peritethyan seas: palaeoclimatic significance inferred from multiproxy comparisons, *Palaeogeography, Palaeoclimatology, Palaeoecology*, **271**, 39–51.

Dericquebourg P. (2016) *Les environnements sédimentaires néogènes enregistreurs des fluctuations climatiques associées aux premiers hominidés est-africains*. PhD thesis, Université de Liège, Liège, Belgium, 178 pp.

Dericquebourg P., Person A., Segalen L., Pickford M., Senut B. & Fagel M. (2015) Environmental significance of Upper Miocene phosphorites at hominid sites in the Lukeino Formation (Tugen Hills, Kenya). *Sedimentary Geology*, **327**, 43–54.

Derry L.A. & France-Lanord C. (1996) Neogene Himalayan weathering history and river $^{87}Sr/^{86}Sr$: impact on the marine Sr record. *Earth Planetary Sciences Letters*, **142**, 59–74.

Dickson R.R. & Brown J. (1994) The production of North Atlantic Deep Water: sources, rates, and pathways. *Journal of Geophysical Research*, **99**, 12319–12341.

Dieckmann B., Kuhn G. & Mackensen A., Petschick R., Fütterer D.K., Gersonde R. *et al.* (1999) Kaolinite and chlorite as tracers of modern and Late Quaternary Deep Water Circulation in the South Atlantic and the adjoining Southern Ocean. Pp. 285–313 in: *Use of Proxies in Paleoceanography – Examples from the South Atlantic* (G. Fischer & G. Wefer, editors). Springer, Berlin, Germany.

Dieckmann B., Petschick R., Gingele F.X., Fütterer D.K., Abelmann A., Brathauer U. *et al.* (1996) Clay mineral fluctuations in Late Quaternary sediments of the southeastern South Atlantic: implications for past changes of deepwater advection. Pp. 621–644 in: *The South Atlantic: Present and Past Circulation*, vol. 118 (G. Wefer, W.H. Berger, G. Siedler & D. Webb, editors). Springer-Verlag, Berlin, Germany.

Dietel J., Ufer K., Kaufhold S. & Dohrmann R. (2019) Crystal structure model development for soil clay minerals – II. Quantification and characterization of hydroxy-interlayered smectite (HIS) using the Rietveld refinement technique. *Geoderma*, **347**, 1–12.

Dunn D.A., Patrick D.M. & Cooley U. (1987) Cenozoic clay mineralogy of Sites 604 and 605, New Jersey Transect, Deep Sea Drilling Project, Leg 93. Pp. 1023–1037 in: *Initial Reports of the Deep Sea Drilling Project*, vol. 93 (J.E. Van Hinte, S.W. Wise Jr, *et al.*, editors). US Government Printing Office, Washington, DC, USA.

Dunoyer de Segonzac G. (1969) Les minéraux argileux dans la diagenèse. Passage au métamorpisme. *Mémoire Service Carte géologique Alsace-Lorraine*, **29**, 1–320.

Eberl D.D. (2003) *User's Guide to* RockJock - *A Program for Determining Quantitative Mineralogy from Powder X-Ray Diffraction Data*. US Geological Survey Open-File Report 2003-78. US Geological Survey, Reston, VA, USA, 47 pp.

Egli M., Merkli C., Sartori G., Mirabella A. & Plötze M. (2008). Weathering, mineralogical evolution and soil organic matter along a Holocene soil

toposequence developed on carbonate-rich materials. *Geomorphology*, **97**, 675–696.

Fagel N. (2007) Marine clay minerals, deep circulation and climate. Pp. 139–184 in: *Paleoceanography of Late Cenozoic, Vol. 1: Methods* (C. Hillaire-Marcel & A. de Vernal, editors). Elsevier, Amsterdam, The Netherlands.

Fagel N. & Boës X. (2008) Clay-mineral record in Lake Baikal sediments: the Holocene and Late Glacial transition. *Palaeogeography, Palaeoclimatology, Palaeoecology*, **259**, 230–243.

Fagel N. & Hillaire-Marcel C. (2006) Glacial/interglacial instabilities of the Western Boundary Undercurrent during the last 360 kyr from Sm/Nd ratios of the sedimentary clay-size fractions at ODP Site 646 (Labrador Sea). *Marine Geology*, **232**, 87–99.

Fagel N. & Mackay A. (2008) Weathering in the Lake Baikal watershed during the Kazantsevo (Eemian) interglacial: evidence from the lacustrine clay record. *Paleogeography, Paleoecology, Paleoclimatology*, **259**, 230–343.

Fagel N., André L., Chamley H., Debrabant P. & Jolivet L. (1992a) Clay sedimentation in the Japan Sea since the Early Miocene: influence of source-rock and hydrothermal activity. *Sedimentary Geology*, **80**, 27–40.

Fagel N., André L. & Debrabant P. (1997a) The geochemistry of pelagic clays: detrital *versus* non-detrital signals? *Geochimica et Cosmochimica Acta*, **61**, 989–1008.

Fagel N., Boski T., Likhoshway L. & Oberhaensli H. (2003) Late Quaternary clay mineral record in Central Siberia Lake Baikal (Academician Ridge, Siberia). *Palaeogeography, Palaeoclimatology, Palaeoecology*, **193**, 159–179.

Fagel N., Debrabant P. & André L. (1994) Clay supplies in the Central Indian Basin since the Late Miocene: climatic or tectonic control? *Marine Geology*, **122**, 151–172.

Fagel N., Debrabant P., De Menocal P. & Demoulin B. (1992b) Utilisation des minéraux sédimentaires argileux pour la reconstitution des variations paléoclimatiques à court terme en Mer d'Arabie. *Oceanologica Acta*, **15**, 125–136 [in French].

Fagel N., Hillaire-Marcel C., Humblet M., Brasseur R., Weis D. & Stevenson R. (2004) Nd and Pb isotope signatures of the clay-size fraction of Labrador Sea sediments during the Holocene: Implications for the inception of the modern deep circulation pattern. *Paleoceanography and Paleoclimatology*, **19**, 10.1029/2003PA000993.

Fagel N., Hillaire-Marcel C. & Robert C. (1997b) Changes in the Western Boundary Undercurrent outflow since the Last Glacial Maximum, from smectite/illite ratios in deep Labrador Sea sediments. *Paleoceanography and Paleoclimatology*, **12**, 79–96.

Fagel N., Innocent C., Gariépy C. & Hillaire-Marcel C. (2002) Sources of Labrador Sea sediments since the last glacial maximum inferred from Nd-Pb isotopes. *Geochimica et Cosmochimica Acta*, **66**, 2569–2581.

Fagel N., Innocent C., Stevenson R.K., Hillaire-Marcel C. (1999) Nd isotopes as tracers of paleocurrents: a high resolution study of Late Quaternary sediments from the Labrador Sea. *Paleoceanography and Paleoclimatology*, **14**, 777–788.

Fagel N., Israde-Alcantara I., Safaierad R., Rantala M., Schmidt S., Lepoint G. *et al.* (2024) Environmental significance of kaolinite variability over the last centuries in crater lake sediments from Central Mexico. *Applied Clay Science*, **247**, 107211.

Fagel N., Not C., Gueibe J., Mattielli N. & Bazhenova E. (2014) Late Quaternary evolution of sediment provenances in the Central Arctic Ocean: mineral assemblage, trace element composition and Nd and Pb isotope fingerprints of detrital fraction from the northern Mendeleev Ridge. *Quaternary Science Review*, **92**, 140–154.

Fagel N., Robert C., Hillaire-Marcel C. (1996) Clay mineral signature of the North Atlantic Boundary Undercurrent. *Marine Geology*, **130**, 19–28.

Fagel N., Thamó-Bózsó E. & Heim B. (2007) Mineralogical signatures of Lake Baikal sediments: sources of sediment supplies through Late Quaternary. *Sedimentary Geology*, **194**, 37–59.

Fletcher B., Brentnall S., Anderson C., Berner R.A. & Beerling D.J. (2008) Atmospheric carbon dioxide linked with Mesozoic and early Cenozoic climate change. *Nature Geoscience*, **1**, 43–48.

Foerster V., Asrat A., Bronk Ramsey C., Brown E.T., Chapot M.S., Deion A. *et al.* (2022) Pleistocene climate variability in eastern Africa influenced hominin evolution. *Nature Geoscience*, **15**, 805–811.

Foerster V., Deocampo D.M., Asrat A. & Günter C. (2018) Towards an understanding of climate proxy formation in the Chew Bahir basin, southern Ethiopian Rift. *Palaeogeography, Palaeoclimatology, Palaeoecology*, **501**, 111–123.

Foerster V., Junginger A., Langkamp O., Gebru T., Asrat A., Umer M. *et al.* (2012) Climatic change recorded in the sediments of the Chew Bahir basin, southern Ethiopia, during the last 45,000 years. *Quaternary International*, **274**, 25–37.

Foerster V., Vogelsang R., Junginger A., Asrat A., Lamb H.F., Schaebitz F. & Trauth M.H. (2015) Environmental change and human occupation of southern Ethiopia and northern Kenya during the last 20,000 years. *Quaternary Science Reviews*, **129**, 333–340.

Foucault A. & Mélières F. (2000) Palaeoclimatic cyclicity in central Mediterranean Pliocene sediments: the mineralogical signal. *Palaeogeography, Palaeoclimatology, Palaeoecology*, **158**, 311–323.

France-Lanord C., Derry L. & Michard A. (1993) Evolution of the Himalaya since Miocene time: isotopic and sedimentological evidence from the Bengal Fan. *Geological Society, London, Special Publications*, **74**, 603–621.

Galasy G.I. (editor) (1993) *Baikal Atlas*. Russian Academy of Science, Siberian Branch. Roskartografiya, Moscow, Russia, 160 pp. [in Russian].

Gates-Rector S. & Blanton T. (2019) The Powder Diffraction File: a quality materials characterization database. *Powder Diffraction*, **34**, 352–360.

Gingele F. & Schmiedl G. (1999) Comparison of independent proxies on deep water advection in the southeast Atlantic off Namibia. *South African Journal of Marine Science*, **21**, 181–190.

Gingele F.X., Schmieder F., von Dobeneck T., Petschick R. & Rühlemann C. (1999) Terrigenous flux in the Rio Grande Rise area during the past 1500 ka: evidence of deep water advection or rapid response to continental rainfall patterns? *Paleoceanography and Paleoclimatology*, **14**, 84–95.

Godet A., Bodin S., Adatte T. & Föllmi K.B. *et al.* (2008) Platform induced clay-mineral fractionation along a northern Tethyan basin-platform transect: implications for the interpretation of Early Cretaceous climate change (Late Hauterivian–Early Aptian). *Cretaceous Research*, **29**, 830–847.

Grachev M.A., Vorobieva S.S. & Likoshway E.V. (1998) A high-resolution diatom record of the paleoclimates of East Siberia for the last 2,5 My from Lake Baikal. *Quaternary Science Reviews*, **17**, 1101–1106.

Griffin J.J. & Goldberg E.D. (1963) Clay mineral distribution in the Pacific Ocean. Pp. 728–741 in: *The Sea* (M.N. Hill, editor). Interscience, New York, NY, USA.

Griffin J.J., Windom H. & Goldberg E.D. (1968) The distribution of clay minerals in the world ocean. *Deep Sea Research*, **15**, 433–459.

Han T.G., Préat A., Chamley H., Deconinck J.-F. & Mansy J.-L. (2000) Palaeozoic clay mineral sedimentation and diagenesis in the Dinant and Avesnes basins (Belgium, France): relationships with Variscan tectonism. *Sedimentary Geology*, **136**, 217–238.

Harms U., Koeberl C. & Zoback M.C. (editors) (2007) *Continental Scientific Drilling: A Decade of Progress, and Challenges for the Future*. Springer-Verlag, Berlin, Germany, 366 pp.

Hays J.D., Imbrie J. & Shackleton N.J. (1976) Variations in Earth's orbit pacemaker of ice ages. *Science*, **194**, 1121–1132.

Hesselbo S.P., Bjerrum C.J., Hinnov L.A., MacNiocaill C., Miller K., Riding J. *et al.* (2013) Mochras borehole revisited: a new global standard for Early Jurassic Earth history. *Scientific Drilling*, **16**, 81–91.

Hesselbo S.P., Hudson A.J.L., Huggett J.M., Leng M.J., Riding J.B. & Ullmann C.V. (2020) Palynological, geochemical, and mineralogical characteristics of the Early Jurassic Liasidium Event in the Cleveland Basin, Yorkshire, UK. *Newsletters on Stratigraphy*, **53**, 191–211.

Hillaire-Marcel C., de Vernal A., Bilodeau C. & Wu G. (1994) Isotope stratigraphy, sedimentation rates, deep circulation, and carbonate events in the Labrador Sea during the last 200 ka. *Canadian Journal of Earth Sciences*, **31**, 139–158.

Hillier S. (1999) Use of an air brush to spray dry samples for X-ray powder diffraction. *Clay Minerals*, **34**, 127–135.

Hillier S. (2000) Accurate quantitative analysis of clay and other minerals in sandstones by XRD: comparison of a Rietveld and a reference intensity ratio (RIR) method and the importance of sample preparation. *Clay Minerals*, **35**, 291–302.

Hillier S., Wilson M.J. & Merriman R.J. (2006) Clay mineralogy of the Old Red Sandstone and Devonian sedimentary rocks of Wales, Scotland and England. *Clay Minerals*, **41**, 433–471.

Holtzapffel T. (1985) *Les minéraux argileux, préparation, analyse diffractométrique et détermination*. Société Géologique du Nord, Publication 12. Société Géologique du Nord, Lille, France.

Horiuchi K., Minoura K., Hoshino K., Oda T., Nakamura T. & Kawai T. (2000) Palaeoenvironmental history of Lake Baikal during the last 23000 years. *Palaeogeography, Palaeoclimatology, Palaeoecology*, **157**, 95–108.

Huang C., Hesselbo S.P. & Hinnov L. (2010) Astrochronology of the late Jurassic Kimmeridge Clay (Dorset, England) and implications for Earth system processes. *Earth and Planetary Science Letters*, **289**, 242–255.

Hutchinson D.R., Golmshtok A.J., Zonenshain L.P., Moore T.C., Scholz C.A. & Klitgord K.D. (1992) Depositional and tectonic framework of the rift basins of Lake Baikal from multichannel seismic data. *Geology*, **21**, 589–592.

ICDD (2016) *PDF-4 + 2016 (Database)*. International Center for Diffraction Data, Newtown Square, PA, USA.

Inoue A. (1995) Formation of clay minerals in hydrothermal environments. Pp. 268–329 in: *Origin and Mineralogy of Clays* (B. Velde, editor). Springer, Berlin, Germany.

Jeans C.V. (2006) Clay mineralogy of the Jurassic strata of the British Isles. *Clay Minerals*, **41**, 187–307.

Jenkins W.M. & Watts D.G. (1968) *Spectral Analysis and Its Application*. Holden-Day, San Francisco, CA, USA, 525 pp.

Johanson D.C., Taieb M. & Coppens Y. (1982) Pliocene hominids from the Hadar Formation, Ethiopia (1973–1977): stratigraphic, chronological, and paleoenvironmental contexts, with notes on hominid morphology and systematics. *American Journal of Physical Anthropology*, **57**, 373–402.

Joussain R., Colin C., Liu Z.F., Meynadier L., Fournier L., Fauquembergue K. *et al.* (2016) Climatic control of sediment transport from the Himalayas to the proximal NE Bengal Fan during the last glacial–interglacial cycle. *Quaternary Science Reviews*, **148**, 1–16.

Karabanov E.B., Prokopenko A.A., Williams D.F. & Khursevich G.K. (2000) Evidence for mid-Eemian cooling in continental climatic record from Lake Baikal. *Journal of Paleolimnology*, **23**, 365–371.

Kaufhold S., Hein M., Dohrmann R. & K. Ufer (2012) Quantification of the mineralogical composition of clays using FTIR spectroscopy. *Vibrational Spectroscopy*, **56**, 29–39.

Kemp S.J., Merriman R.J. & Bouch J.E. (2005) Clay mineral reaction progress – the maturity and burial history of the Lias Group of England and Wales. *Clay Minerals*, **40**, 43–61.

Kennett J.P. (1982) *Marine Geology*. Prentice Hall, Englewood Cliffs, NJ, USA, 813 pp.

Khotinsky N.A. (1984) Holocene vegetation history. Pp. 179–200 in: *Late Quaternary Environments of the Soviet Union* (AA. Velichko, editor). University of Minnesota Press, Minneapolis, MN, USA.

Kolla V. & Rao N.M. (1990) Sedimentary sources in the surface and near-surface sediments of the Bay of Bengal. *Geo-Marine Letters*, **10**, 129–136.

Kolla V., Henderson L. & Biscaye P.E. (1976) Clay mineralogy and sedimentation in the western Indian Ocean. *Deep Sea Research*, **23**, 949–961.

Korte C., Hesselbo S.P., Ullmann C., Dietl G., Ruhl M., Schweigert G. & Thibault N. (2015) Jurassic climate mode governed by ocean gateway. *Nature Communi*cation, **6**, 1–7.

Krissek L.A. & Clemens S.C. (1991). Mineralogic variations in a Pleistocene high resolution eolian record from the Owen Ridge Western Arabian Sea (Site 722): implications for sediment source conditions and monsoon history. Pp. 197–213 in: *Proceedings of the Ocean Drilling Program. Scientific Results* (W.L. Prell, N. Niitsuma, K.-C. Emeis, Z.K. Al-Sulaiman, A.N.K. Al-Tobbah, D.M. Anderson *et al.*, editors), **117**. Ocean Drilling Program, College Station, TX, USA.

Kutzbach J.E. (1981) Monsoon climate of the early Holocene: climate experiment with the Earth's orbital parameters for 9000 years ago. *Science*, **214**, 59–61.

Kuzmin M.I., Karabanov E.B., Kawai T. & Williams D. (2001) Deep drilling on Lake Baikal: main results. *Russian Geology and Geophysics*, **42**, 8–34.

Lamy F., Hebbeln D. & Wefer G. (1999) High resolution marine record of climatic change in midlatitude Chile during the last 28,000 years based on terrigenous sediment parameters. *Quaternary Research*, **51**, 83–93.

Landwehrs J., Feulner G., Petri S., Sames B. & Wagreich M. (2021) Investigating Mesozoic climate trends and sensitivities with a large ensemble of climate model simulations. *Paleoceanography and Paleoclimatology*, **36**, e2020PA004134.

Laskar J., Fienga A., Gastineau M. & Manche H. (2011) La2010: a new orbital solution for the long-term motion of the Earth. *Astronomy & Astrophysics*, **532**, A89.

Last W.M. (2004) Mineralogical analysis of lake sediments. Pp. 143–187 in: *Tracking Environmental Change Using Lake Sediments*. Physical and Geochemical Methods, vol. 2 (W.M. Last & J.P. Smol, editors). Kluwer Academic Publishers, Dordrecht, The Netherlands.

Ledbetter M.T. & Balsam W.M. (1985) Paleoceanography of the Deep Western Boundary Undercurrrent on the North American continental margin for the past 25,000 yr. *Geology*, **13**, 181–184.

Li J., Liu S., Shi X., Zhang H., Fang X., Chen M.-T. *et al.* (2018) Clay minerals and Sr-Nd isotopic composition of the Bay of Bengal sediments: implications for sediment provenance and climate control since 40 ka. *Quaternary International*, **493**, 50–58.

Likhoshway Y.V. (1998) Fossil endemic centric diatoms from Lake Baikal. Upper Pleistocene complexes. Pp. 613–628 in: *Proceedings of the 14th International Diatom Symposium 1996* (S. Manami, M. Idei & I. Koizumi, editors). Koeltz Science Books, Koenigstein, Germany.

Liu Z., Colin C., Li X., Zhao Y., Tuo S., Chen Z. *et al.* (2010) Clay mineral distribution in surface sediments of the northeastern South China Sea and surrounding fluvial drainage basins: source and transport. *Marine Geology*, **277**, 48–60.

Liu Z., Trentesaux A., Clemens S.C., Colin C., Wang P., Huang B. & Boulay S. (2003) Clay mineral assemblages in the northern South China Sea: implications for East Asian monsoon evolution over the past 2 million years. *Marine Geology*, **201**, 133–146.

Lomonosov I.S., Khaustov A.P.K., Gvozdkov A.N. & Shpeizer G.M. (1995) Geochemical significance of substance flows in recent sedimentation of Lake Baikal. *IPPCCE Newsletter*, **9**, 57–65.

Lourens L., Hilgen F., Laskar J. & Wilson D. (2005) The Neogene period. Pp. 409–440 in: *A Geological Timescale 2004* (F. Gradstein, J. Ogg & A. Smith, editors). Cambridge University Press, Cambridge, UK.

Lucotte M. & Hillaire-Marcel C. (1994) Identification des grandes masses d'eau dans les mers du Labrador et d'Irminger. *Canadian Journal of Earth Sciences*, **31**, 5–13.

Lupien R., Uno K., Rose C., deRoberts N., Hazan C., de Menocal P. & Polissar P. (2023) Low-frequency orbital variations controlled climatic and environmental cycles, amplitudes, and trends in northeast Africa during the Plio-Pleistocene. *Communications Earth and Environment*, **4**, 360.

Martinez M., Pellenard P., Deconinck J.F., Monna F., Riquier L. Boulila S., *et al.* (2012) An orbital floating time scale of the Hauterivian/Barremian GSSP from a magnetic susceptibility signal (Río Argos, Spain). *Cretaceous Research*, **36**, 106–115.

Martinson D.G., Pisias N.G., Hays J.D., Imbrie J., Moore T. & Shackleton N.J. (1987) Age dating and the orbital theory of the ice ages: development of a high resolution 0 to 300,000-year chronostratigraphy. *Quaternary Research*, **27**, 1–29.

Mats V., Khlystov O., De Batist M., Ceramicola S., Lomonosova T.K. & Klimansky A. (2000) Evolution of the Academician Ridge Accommodation Zone in the central part of the Baikal Rift, from high-resolution reflection seismic profiling and geological field investigations. *International Journal of Earth Sciences*, **89**, 229–250.

McCartney M.S. (1992) Recirculating components to the deep boundary current of the northern North Atlantic. *Progress in Oceanography*, **29**, 283–383.

McCarty D.K. (2002) Quantitative mineral analysis of clay-bearing mixtures: the 'Reynolds Cup' contest. *Committee on Powder Diffraction Newsletter*, **27**, 12–16,

Melles M., Grobe H. & Hubberten H.W. (1995) Mineral composition of the clay fraction in the 100 m Core BDP-93-2 from Lake Baikal – preliminary results. In: Horie S. (Ed.), *IPPCC Newsletter* **9**, 17–22.

Meunier A. (2006) *Clays*. Springer-Verlag, Berlin, Germany, 472 pp.

Meunier A. (2007) Soil hydroxy-interlayered minerals: a re-interpretation of their crystallochemical properties. *Clays and Clay Minerals*, **55**, 380–388.

Meyers S.R. (2015) The evaluation of eccentricity-related amplitude modulation and bundling in paleoclimate data: an inverse approach for astrochronologic testing and time scale optimization. *Paleoceanography and Paleoclimatology*, **30**, 1625–1640.

Milliman J.D. & Syvitski J.P.M. (1992) Geomorphic/tectonic control of sediment discharge to the ocean: the importance of small mountainous rivers. *Journal of Geology*, **100**, 525–544

Millot G. (1970) *Geology of Clays: Alteration, Sedimentology, Geochemistry*. Springer Verlag, New York, NY, USA; Masson, Paris, France; Chapman Hill, London, UK, 429 pp.

Moore D.M. & Reynolds R.C. (1997) *X-Ray Diffraction and the Identification and Analysis of Clay Minerals*. Oxford University Press, Oxford, UK, 332 pp.

Müller J., Kasbohm J., Oberhaensli H., Melles M. & Hubberten H.W. (2000) TEM analysis of smectite–illite mixed-layer minerals of core BDP96 Hole 1: preliminary results. Pp. 90–100 in: *Lake Baikal: A Mirror in Time and Space for Understanding Global Change Processes* (K. Minoura, editor). Elsevier, Amsterdam, The Netherlands.

Munier T., Deconinck J.F., Pellenard P., Hesselbo S.P., Riding J.B., Ullmann C.V. *et al.* (2021) Million-year-scale alternation of warm–humid and semi-arid periods as a mid-latitude climate mode in the Early Jurassic (late Sinemurian, Laurasian Seaway). *Climate of the Past*, **17**, 1547–1566.

Nair R.R., Ittekkot V., Manganini S.J., Ramaswamy V., Haake B., Degens E.T. *et al.* (1989) Increased particle flux to the deep ocean related to monsoons. *Nature*, **338**, 749–751.

Nath B.N., Rao V.P. & Becker K.P. (1989) Geochemical evidence of terrigenous influence in deep-sea sediments up to 8°S in the Central Indian Basin. *Marine Geology*, **87**, 301–313.

Nesje A. & Dahl. S.O. (2000) *Glaciers and Environmental Changes. Key Issues in Environmental Change*. Routledge, London, UK 216 pp.

Omotoso O., McCarty D.K., Hillier S. & Kleeberg R. (2006) Some successful approaches to quantitative mineral analysis as revealed by the 3rd Reynolds Cup contest. *Clays and Clay Minerals*, **54**, 748–760.

Oppo J., McManus F. & Cullen J.L. (2003) Deepwater variability in the Holocene epoch. *Nature*, **277**, 422.

Peacor D.R. (1992) Diagenesis and low-grade metamorphism of shales and slates. Pp. 335–380 in: *Minerals and Reactions at the Atomic Scale: Transmission Electron Microscopy* (P.R. Busek, editor). Mineralogical Society of America, Chantilly, VA, USA.

Pellenard P. & Deconinck J.F. (2006) Mineralogical variability of Callovo–Oxfordian clays from the Paris Basin and the Subalpine Basin. *Comptes Rendus Geoscience*, **338**, 854–866.

Perry E. & Hower J. (1970) Burial diagenesis in Gulf Coast pelitic sediments. *Clays and Clay Minerals* **18**, 165–178.

Petschick R. (1997) Powder Diffraction Software. *MacDiff* [Online]. Retrieved from: http://mill2.chem.ucl.ac.uk/ccp/web-mirrors/krumm/macsoftware/macdiff/macdiff4.html

Petschick R., Kuhn G. & Gingele F. (1996) Clay mineral distribution in surface sediments of the South Atlantic: sources, transport, and relation to oceanography. *Marine Geology*, **130**, 203–229.

Pickford M. (1974) *Stratigraphy and paleoecology of five late Cenozoic formations in the Kenya Rift Valley*. Unpublished PhD Thesis. University of London, London, UK, 219 pp.

Pickford M. (1975) Miocene sediments and fossils from the northern Kenya Rift Valley. *Nature*, **256**, 279–284.

Pickford M. (1978) Stratigraphy and mammalian palaeontology of the late-Miocene Lukeino Formation, Kenya. Pp. 263–278 in: *Geological Background to Fossil Man* (W.W. Bishop, editor). Scottish Academic Press, Edinburgh, UK.

Pickford M., Senut B. & Cheboi K. (2009) The geology and palaeobiology of the Tugen Hills, Kenya: rift tectonics, basin formation, volcanics and sedimentation. *Geo-Pal Kenya*, **1**, 4–133.

Piper D.J.W. & Slatt R.M. (1977) Late Quaternary clay mineral distribution on the eastern continental margin of Canada. *GSA Bulletin*, **88**, 267–272.

Prell W.L. (1984) Monsoonal climate of the Arabian Sea during the late Quaternary: a response to changing solar radiation. Pp. 349–366 in: *Milankovitch and Climate (Pt. 1)* (A.L. Berger, J. Imbrie, J. Hayse, G. Kukla & B. Saltzman, editors). D. Reidel, Dordrecht, The Netherlands.

Prell W.L. & Kutzbach J.E. (1987) Monsoon variability over the past 150,000 years. *Journal of Geophysical Research*, **92**, 8411–8525.

Prell W.L. & Van Campo E. (1986) Coherent response of Arabian Sea upwelling and pollen transport to late Quaternary monsoonal winds. *Nature*, **323**, 526–528.

Press W.H., Flannery B.P., Teukolsky S.A. & Vetterling W.T. (1986) *Numerical Recipes: The Art of Scientific Computing*. Cambridge University Press, Cambridge, UK, 818 pp.

Prokopenko A.A., Karabanov E.B., Williams D.F. & Khursevich G.K. (2002) The stability and the abrupt ending of the Last Interglaciation in southeastern Siberia. *Quaternary Research*, **58**, 56–59.

Rateev M.A., Gorbunova Z.N., Lisitzyn A.P. & Nosov G.L. (1969) The distribution of clay minerals in the oceans. *Sedimentology*, **13**, 21–43.

Raven M.D. & Self P.G. (2017) Outcomes of 12 years of the Reynolds Cup quantitative minerals analysis round robin. *Clays and Clay Minerals*, **65**, 122.

Reed K.E. (2008) Paleoecological patterns at the Hadar hominin site, Afar Regional State, Ethiopia. *Journal of Human Evolution*, **54**, 743–768.

Rich C.I. (1968) Hydroxy-interlayers in expansible layer silicates. *Clays and Clay Minerals*, **16**, 15–30.

Rietveld H.M. (1967) Line profiles of neutron powder-diffraction peaks for structure refinement. *Acta Crystallographica*, **22**, 151–152.

Rietveld H.M. (1969) A profile refinement method for nuclear and magnetic structures. *Journal of Applied Crystallography*, **2**, 65–71.

Robert C., Diester-Haass L. & Paturel J. (2005) Clay mineral assemblages, siliciclastic input and paleoproductivity at ODP Site 1085 off southwest Africa: a late Miocene–early Pliocene history of Orange river discharges and Benguela current activity, and their relation to global sea level change. *Marine Geology*, **216**, 221–238.

Roche D., Ségalen L., Senut B. & Pickford M. (2013) Stable isotope analyses of tooth enamel carbonates of large herbivores from the Tugen Hills deposits: palaeoenvironmental context of the earliest Kenyan hominids. *Earth Planetary Sciences Letters*, **381**, 39–51.

Ruddiman W.F. & McIntyre A. (1981) Oceanic mechanisms for amplification of the 23,000 years ice volume cycle. *Science*, **212**, 617–627.

Ruffell A., McKinley J.M. & Worden R.H. (2002) Comparison of clay mineral stratigraphy to other proxy palaeoclimate indicators in the Mesozoic of NW Europe. *Philosophical Transactions of the Royal Society A*, **360**, 675–693.

Sakai T., Minoura K., Soma M., Tani Y., Tanaka A., Nara F., *et al.* (2005) Influence of climate fluctuation on clay formation in the Baikal drainage basin. *Journal of Paleolimnology*, **33**, 105–121.

Sawada Y., Pickford M., Senut B., Itaya T., Hyodo M., Miura T. *et al.* (2002) The age of *Orrorin tugenensis*, an early hominid from the Tugen Hills, Kenya. *Comptes Rendus Palevol*, **1**, 293–303.

Schirrmeister L., Siegert C. & Kuznetsova T. (2002) Paleoenvironmental and paleoclimatic records from permafrost deposits in the Arctic region of northern Siberia. *Quaternary International*, **89**, 97–118.

Schlunegger F. & Norton K.P. (2015) Climate vs. tectonics: the competing roles of Late Oligocene warming and Alpine orogenesis in constructing alluvial megafan sequences in the North Alpine foreland basin. *Basin Research*, **27**, 230–245.

Schnyder J., Ruffell A., Deconinck J.F. & Baudin F. (2006) Conjunctive use of spectral gamma-ray logs and clay mineralogy in defining late Jurassic–early Cretaceous palaeoclimate change (Dorset, U.K.). *Palaeogeography,. Palaeoclimatology, Palaeoecology*, **229**, 303–320.

Senut B., Pickford M., Gommery D., Mein P., Cheboi K. & Coppens Y. (2001) First hominid from the Miocene (Lukeino Formation, Kenya). *Comptes Rendus de l'Académie des Sciences de Paris-Series IIA, Earth and Planetary Sciences*, **332**, 137–144.

Shackleton N.J., Backmann H.B., Zimmerman H.B., Kent D.V., Hall M.A., Roberts D.G. *et al.* (1984) Oxygen isotope calibration of the onsert of ice-rafteing in DSDP Site 552°: history of glaciaition in the North Atlantic region. *Nature*, **307**, 620–623.

Shackleton N.J., Berger A. & Peltier W.R. (1990) An alternative astronomical calibration of the lower Pleistocene timescale based on ODP Site 677. *Earth and Environmental Science Transactions of the Royal Society of Edinburgh*, **81**, 251–261.

Singer A. (1984) The paleoclimatic interpretation of clay minerals in sediments. *Earth Science Review*, **21**, 251–293.

Snyder R.L. & Bish D.L. (1989) *Modern Powder Diffraction*. Mineralogical Society of America. *Reviews in Mineralogy*, **20**, 101–144.
Solotchina E.P., Prokopenko A.A., Vasilevsky A.N., Gavshin V.M., Kuzmin M.I. & Williams D.F. (2002) Simulation of XRD patterns as an optimal technique for studying glacial and interglacial clay mineral associations in bottom sediments of Lake Baikal. *Clay Minerals*, **37**, 105–119.
Srivastava S.P., Arthur M., Clement B., Aksu A., Baldauf J., Bohrmann G. *et al.* (1987) *Proceedings of the Ocean Drilling Program, Initial Report*, vol. 105. Ocean Drilling Program, College Station, TX, USA.
Srivastava P., Parkash B. & Pal D.K. (1998) Clay minerals in soils as evidence of Holocene climatic central Indo-Gangetic Plains, north-central India. *Quaternary Research*, **50**, 230–239.
Środoń J. (2003) Identification and quantitative analysis of clay minerals. Pp. 765–787 in: *Handbook of Clay Science* (F. Bergaya, B.K.G. Theng & G. Lagaly, editors). Developments in Clay Science, vol. 1. Elsevier, Amsterdam, The Netherlands.
Środoń J., Drits V.A., McCarty D.K., Hsieh J.C.C. & Eberl D.D. (2001) Quantitative X-ray diffraction analysis of clay-bearing rocks from random preparations. *Clays and Clay Minerals*, **49**, 514–528.
Stein S. & Okal E.A. (1978) Seismicity and tectonics of the Ninety East Ridge area: evidence for internal deformation of the Indian plate. *Journal of Geophysical Research*, **83**, 2233–2245.
Tiercelin J.J. & Lezzar K.E. (2002) A 300 million years history of rift lakes in Central and East Africa: an updated broad review. Pp. 3–60 in: *The East African Great Lakes: Limnology, Paleolimnology and Biodiversity* (E.O. Odada & D.O. Olgado, editors). Advances in Global Change Research, vol. 12. Springer, Berlin, Germany.
Thiry M. (2000) Palaeoclimatic interpretation of clay minerals in marine deposits: an outlook from the continental margin. *Earth Sciences Review*, **49**, 201–221.
Thorez J. (1976) *Practical Identification of Clay Minerals*. G. Lelotte (editor). Lelotte, Dison, Belgique, 90 p.
Thorez J. (1998) Différienciation minéralogique et génétique par DRX des smectites post-saturées au Li et K. Pp. 106–107 in: *Réunion spécialisée ASF-SGF. Lille, 20–21/11*/1998, vol. 30. ASF Publications, Paris, France.
Thorez J. (2000) Cation-saturated swelling physils: an XRD revisitation. *Proceedings of the 1st Latin-American Clay Conference, Funchal, Madeira*, I, 71–85.
Trentesaux A., Liu Z., Colin C., Boulay S. & Wang P. (2003) Data report: Pleistocene paleoclimatic cyclicity of southern China: clay mineral evidence recorded in the South China Sea (ODP Site 1146). Pp 1–10 in: *Proceedings of the Ocean Drilling Program, Scientific Results* (W.L. Prell, P. Wang, P. Blum, D.K. Rea & S.C. Clemens, editors), vol. 184. Ocean Drilling Program, College Station, TX, USA.
Ufer K., Kleeberg R., Bergmann J. & Dohrmann R. (2012) Rietveld refinement of disordered illite-smectite mixed-layer structures by a recursive algorithm. II: Powder pattern refinement and quantitative phase analysis. *Clays and Clay Minerals*, **60**, 535–552.
Ufer K., Stanjek H., Roth G., Dohrmann R., Kleeberg R. & Kaufhold S. (2008) Quantitative phase analysis of bentonites by the Rietveld method. *Clays and Clay Minerals*, **56**, 272–282.
Vanderaveroet P., Averbuch O., Deconinck J.F. & Chamley H. (1999) A record of glacial–interglacial alternations in Pleistocene sediments off New Jersey expressed by clay mineral, grain size and magnetic susceptibility data. *Marine Geology*, **159**, 79–92.
Vanderaveroet P., Bout-Roumazeilles, Fagel N., Chamley H. & Deconinck J.F. (2000) Significance of random illite–vermiculite mixed layers in Pleistocene sediments of the northwestern Atlantic Ocean. *Clay Minerals*, **35**, 679–691.
Velde B. (1992) *Introduction to Clay Minerals*. Chapman and Hall, London, UK, 198 pp.
Venkatarathnam K. & Biscaye P.E. (1973) Clay mineralogy and sedimentation in the eastern Indian Ocean. *Deep Sea Research*, **20**, 727–738.
Vorobyova G.A. (1994) Paleoclimates around Lake Baikal in Pleistocene and the Holocene. Pp. 54–55 in: *Baikal as a Natural Laboratory for Global Change*, vol. 2. Lisna Publishers, Irkutsk, Russia.
Wang B., Clemens S.C. & Liu P. (2003) Contrasting the Indian and East Asian monsoons: implications on geological timescales. *Marine Geology*, **201**, 5–21.
Wang L. & Wang P. (1990) Late Quaternary paleoceanography of the South China Sea: glacial–interglacial contrasts in an enclosed basin. *Paleoceanography and Paleoclimatology*, **5**, 77–90.
Wang P., Wang L., Bian Y. & Jian Z. (1995) Late Quaternary paleoceanography of the South China Sea: surface circulation and carbonate cycles. *Marine Geology*, **127**, 145–165.
Warr L.N. (2022) Earth's clay mineral inventory and its climate interaction: a quantitative assessment. *Earth Science Review*, **234**, 104198.
Weber M.E., Wiedicke M.H., Kudrass H.R., Hübscher C. & Erlenkeuser H. (1997) Active growth of the Bengal Fan during sea-level rise and highstand. *Geology*, **25**, 315–318.
Webster P.J. (1987) The elementary monsoon. Pp. 3–32 in: *Monsoons* (J.S. Fein & P.L. Stephens, editors). John Wiley and Sons, New York, NY, USA.
Weedon G.P. (2003) *Time-Series Analysis and Cyclostratigraphy*. Cambridge University Press, Cambridge, UK, 274 pp.
Williams D.F., Peck J., Karabanov E.B., Prokopenko A.A., Kravchinsky V., King J. & Kuzmin M.I. (1997) Lake Baikal record of continental climate response to orbital insolation during the past 5 million years. *Science*, **278**, 1114–1117.
Windom H.L. (1976) Lithogenous material in marine sediments. *Chemical Oceanography*, **5**, 103–135.
Yemane K., Robert C. & Bonnefile R. (1987) Pollen and clay assemblages of a Late Miocene lacustrine sequence from the northwestern Ethiopian highlands. *Palaeogeography, Palaeoclimatology, Palaeoecology*, **60**, 123–141.
Yuretich R. & Ervin C.R. (2002) Clay minerals as paleoenvironmental indicators in two large lakes of the African Rift Valleys: Lake Malawi and Lake Turkana. Pp. 221–232 in: *Sedimentation in Continental Rifts* (R.W. Renaut & G.M. Ashley, editors). SEPM Special Publication, vol. 73. SEPM Society for Sedimentary Geology, Claremore, OK, USA.
Yuretich R., Melles M., Sarata B. & Grobe H. (1999) Clay minerals in the sediments of Lake Baikal: a useful climate proxy. *Journal of Sedimentary Research*, **69**, 588–596.
Zachos J., Pagani M., Sloan L., Thomas E. & Billups K. (2001) Trends, rhythms, and aberrations in global climate 65 Ma to present. *Science*, **210**, 682–693.
Zeng M.X, Song Y.G., An Z.S., Chang H. & Li Y. (2014) Clay mineral records of the Erlangjian drill core sediments from the Lake Qinghai Basin, China. *Science China: Earth Sciences*, **57**, 1846–1859.
Zhao Y., Colin C., Liu Z., Bonneau L. & Siani S. (2016) Climate forcing of terrigenous sediment input to the central Mediterranean Sea since the early Pleistocene. *Palaeogeography, Palaeoclimatology, Palaeoecology*, **442**, 23–35.
Zhao Y., Colin C., Liu Z., Paterne M., Siani G. & Xie X. (2012) Reconstructing precipitation changes in northeastern Africa during the Quaternary by clay mineralogical and geochemical investigations of Nile deep-sea fan sediments. *Quaternary Sciences Review*, **57**, 58–70.
Zimmerman H.B. (1982) Fine-grained sediment distribution in the late Pleistocene/Holocene North Atlantic. *Bulletin. Institut de Géologie du Bassin d'Aquitaine*, **31**, 337–357.

Websites

Baikal Drilling Program (BDP), https://www.icdp-online.org/projects/by-continent/asia/bdp-russia/
Deep-Sea Drillings Projects (DSDP), http://deepseadrilling.org/
Hominin Sites and Paleolakes Drilling Project (HSPDP), https://www.icdp-online.org/projects/by-continent/africa/hspdp-ethiopia/
International Continental Scientific Drilling Program (ICDP), https://www.icdp-online.org/projects
International Ocean Drilling Projects (IODP), https://www.iodp.org/
Ocean Drilling Projects (ODP), 1983–2007, http://www-odp.tamu.edu/
Profex, Creative Commons Attribution-NonCommercial 4.0 International License by Nicola Doebelin, https://www.profex-xrd.org/lecture-handouts/